



Contents lists available at ScienceDirect

Arabian Journal of Chemistry

journal homepage: www.ksu.edu.sa

Original article

Exploring the mechanism and key active components of Gegen Qinlian decoction combined with XELOX in the treatment of ulcerative colitis-associated colorectal cancer based on network pharmacology and multi-omics analysis

Qi Tang^a, Juan Xie^b, Xinran Jiang^a, Mingming Wang^a, Wei Guo^a, Chen Liang^a, Xin Jiang^a, Qing Li^{a,*}

^a School of Pharmacy, Shenyang Pharmaceutical University, 103 Wenhua Road, Shenyang 110016, China

^b School of Pharmaceutical Sciences, Southern Medical University, No.1023 South Shatai Road, Guangzhou 510515, China

ARTICLE INFO

Keywords:

Ulcerative colitis
Colorectal cancer
XELOX
Gegen Qinlian decoction
Therapeutic mechanism

ABSTRACT

Ulcerative colitis (UC) is an autoimmune disease with a steady increase in global prevalence and long-term susceptibility to colorectal cancer (CRC). CRC is often treated with XELOX regimen (oxaliplatin and capecitabine), which is limited by the high toxicity, many adverse reactions and intolerance of patients, thus often leading to termination of chemotherapy. Traditional Chinese medicine is effective in improving patients' clinical symptoms. Gegen Qinlian decoction (GQD) is frequently utilized in the management of UC and has the potential to treat CRC. Whereas, there are few studies on GQD in the treatment of UC-associated CRC, and the therapeutic mechanism of GQD combined with XELOX has not been fully reported. Herein, HPLC-Q-TOF-MS/MS technique was used to analyze the main chemical components of GQD. Network pharmacology was performed to unveil the critical genes and components of GQD against UC and UC-associated CRC. The detection of TNF- α , IL-1 β , IL-6, VEGF, SOD, MDA and immune factors revealed that GQD played a key role in improving immune function, reducing inflammation and resisting oxidative stress. 16S rDNA sequencing technology results showed that GQD could maintain gastrointestinal homeostasis by increasing beneficial bacteria and decreasing harmful bacteria. Then, metabolomics based on HPLC-Q-TOF-MS/MS found that the combination of GQD and XELOX could significantly restore the disturbance of metabolites. Particularly, the compound-reaction-gene-enzyme network was first constructed to realize the combination of network pharmacology and metabolomics. The results showed that GQD may assist XELOX to play a synergistic anti-tumor role by regulating the key enzymes ALOX15, CYP1B1 and PTGS2 in unsaturated fatty acid metabolism. Finally, the mechanism was verified by western blot, and the key pharmacodynamic components were found by molecular docking. Overall, the current study offered fresh perspectives on both the prevention and treatment of UC to CRC as well as fresh concepts for the therapeutic application of GQD with XELOX to lessen the side effects of chemotherapy and enhance patients' quality of life.

1. Introduction

Ulcerative colitis (UC) is an autoimmune disease that mostly affects the mucosal layer of the colon and rectum (Loftus, 2005, Ordas et al., 2012). In recent years, UC is recognized as a disease that poses a threat to global health due to its recurrence (Zhu et al., 2019). Notably, prolonged UC is a risk factor of colorectal cancer (CRC) (Grivennikov, 2013, Rutter and Riddell, 2014). According to prior studies, individuals with UC had a 2.4 times higher risk of getting CRC compared to healthy

population, and the risk for CRC in UC patients was around 30 % after 35 years (Eaden et al., 2001, Rogler, 2014). With a huge global prevalence (approximately 1.9 million new cases in 2020) and high mortality (0.9 million deaths in 2020), CRC is the second most common cancer in women and the third most prevalent cancer in men (Siegel et al., 2022). The transformation of UC into CRC may impose more heavy economic burden on families and society (Zhu et al., 2017). Therefore, a full understanding of the pathogenesis of UC-induced CRC is essential for the prevention and treatment of progression of disease as well as the

* Corresponding author.

E-mail address: lqyxm@hotmail.com (Q. Li).

<https://doi.org/10.1016/j.arabjc.2024.105625>

Received 27 November 2023; Accepted 9 January 2024

Available online 17 January 2024

1878-5352/© 2024 The Author(s). Published by Elsevier B.V. on behalf of King Saud University. This is an open access article under the CC BY-NC-ND license (<http://creativecommons.org/licenses/by-nc-nd/4.0/>).

optimization of existing treatments.

The combination therapy of oxaliplatin and capecitabine (also known as XELOX method) is one of the most commonly used chemotherapy regimens in the treatment of CRC (Shinji et al., 2022). However, XELOX therapy can produce multiple adverse reactions such as nausea, vomiting, immune function decline, and dose involvement may cause serious neurotoxicity, thereby reducing patients' tolerance and compliance, and eventually leading to the termination of chemotherapy and affecting chemotherapy efficacy (Rodriguez et al., 2017, Quidde et al., 2018). Consequently, there remains an urgent need for exploring a new chemotherapeutic synergistic drug, reducing the dose of chemotherapy drugs or shortening the chemotherapy cycle on the premise of maintaining the chemotherapy effect, in order to enhance patients' quality of life and reduce toxicity and harmful effects brought by XELOX. In clinical practice, traditional Chinese medicine is frequently used in conjunction with chemotherapy medications because of its invaluable benefits for symptom relief, immune system regulation, and overall quality of life (Luo et al., 2019, Sun et al., 2021). As a traditional Chinese medicine, Gegen Qinlian decoction (GQD) contains the following ingredients: Pueraria lobata (Willd.) Ohwi (Gegen), Scutellaria baicalensis Georgi (Huangqin), Coptis chinensis French (Huanglian) and Glycyrrhiza uralensis Fisch (Gancao). The properties of GQD include anti-inflammatory, analgesic, antiviral, antibacterial, antioxidant, and intestinal mucosa protection (Liu et al., 2019, Cao et al., 2021, Li et al., 2021a, Li et al., 2021b). For thousands of years, this conventional medication has been extensively used to treat UC and diarrhea (Xu et al., 2021). In modern research, it has also been used to treat CRC with satisfactory results (Wang et al., 2021). However, although the therapeutic effect of GQD has been reported, its molecular mechanism of action and pharmacological are still not clearly understood. Moreover, the therapeutic effect and mechanism of GQD combined with XELOX therapy have rarely been elucidated.

Network pharmacology provides potent tools for exploring the action mechanism of conventional Chinese formulations (Shi et al., 2022). In order to identify the crucial genes and components that contribute to the pathogenesis of GQD against UC and UC-associated CRC, network pharmacology was performed in the current investigation. TNF- α , IL-1 β , IL-6, VEGF, SOD, MDA and immune factors detected by Elisa and flow cytometry revealed that GQD may treat UC and CRC by enhancing the immunomodulatory functions, anti-inflammatory and anti-tumor. As gastrointestinal diseases, UC and CRC can not only cause significant changes in the above indicators, but also cause disturbances in the structure of gut microbiota. Gut microbiota is a general term of microorganisms in the gut of organisms (Miyachi et al., 2020, Zheng et al., 2020), which participate in the physiological processes such as immune and metabolic regulation and energy supply (Nishida et al., 2018). The structural imbalance of intestinal microflora often leads to numerous gastrointestinal diseases, so maintaining normal intestinal microflora is of great significance to body health (Khan et al., 2019). Accordingly, in the prevention and treatment of UC-associated CRC, altering gut microbiota and metabolites might be a promising therapeutic approach. 16S rDNA sequencing results revealed that widespread dysbiosis in the gut microbiota resulted from the development of UC to CRC, and inflammatory pathology was reduced by GQD through modifying the gut microbiota. After GQD intervention, the abundance of beneficial bacteria such as *Lactobacillus* was significantly increased, while the abundance of harmful bacteria such as *Escherichia-Shigella* was effectively inhibited, which confirmed the hypothesis that GQD could regulate body health by maintaining the homeostasis of intestinal microflora. Metabolomics studies evaluated changes in the metabolic pathway during the evolution of UC to CRC, the intervention of GQD combined with XELOX could enhance the rollback effect on differential metabolite concentrations. Spearman correlation analysis found that the changes of different bacteria genera were correlated with the improvement of metabolic indexes. This finding indicated that GQD improved the metabolic disorders such as unsaturated fatty acids by regulating

intestinal microflora. Moreover, integrated analysis of metabolomics and network pharmacology predicted that GQD might assist XELOX in playing an anti-tumor role by regulating the metabolic pathway of unsaturated fatty acids through ALOX15, CYP1B1 and PTGS2, and the reliability of this hypothesis were then proved by western blot and molecular docking. Ononin, genistein, puerarin, daidzein, skullcap-flavone II, baicalin, wogonoside, p-coumaric acid, coptisine, isoliquiritigenin and glyasperin A were the key active ingredients of GQD.

Taken together, network pharmacology, molecular pharmacology, high-throughput sequencing technology and metabolomics data were integrated in our study to fully confirm that GQD can prevent the transition from UC to CRC. The most important thing is that the action mechanism, pharmacodynamic effect and pharmacodynamic compositional basis of XELOX with GQD in the treatment of UC-associated CRC were systematically and deeply studied for the first time. Our current study not only paved the way for the prevention and treatment from UC to CRC, but also provided scientific basis for new clinical therapies to against CRC based on GQD.

2. Materials and methods

2.1. Reagents and drug preparation

1,2-dimethylhydrazine (DMH), 2,4,6-trinitrobenzenesulfonic acid (TNBS) were obtained from Sigma-Aldrich (St. Louis, MO, USA). Distilled water was got from Wahaha Group Co. Ltd. (Hangzhou, China). Ethanol, pentobarbital sodium and physiological saline were obtained from Yuwang Co. Ltd (Shandong, China). Methanol, formic acid and acetonitrile were purchased from Fisher Scientific (New Jersey, USA). The ELISA kit (TNF- α , VEGF, IL-6, SOD, IL-10, MDA, IL-1 β) was purchased from Shanghai MLBio Biotechnology Co., Ltd. (Shanghai, China). Oxaliplatin and capecitabine was obtained from Qilu Pharmaceutical Co., Ltd (Shandong, China). Protein for Western blot: ALOX15 (ab244205, Abcam), CYP1B1 (ab185954, Abcam), PTGS2 (ab179800, Abcam); Secondary antibody (bs-40295G-HRP; Biomass), rapid blocking solution (Genefist, Oxfordshire, UK).

According to the prescription ratio (8:3:3:2), Pueraria lobata (Willd.) Ohwi (Gegen), Scutellaria baicalensis Georgi (Huangqin), Coptis chinensis French (Huanglian) and Glycyrrhiza uralensis Fisch (Gancao) were immersed in 8 times amount of water for 30 min. First, Pueraria lobata (Willd.) Ohwi (Gegen) was boiled for 20 min. Next, the remaining medicine was boiled (40 min) for twice and filtered through a 200-mesh screen. Then, the two filtrates were combined and concentrated under pressure at 50 °C. GQD was administered to rats at 2.16 g/kg (low dose, equivalent to half of the dose of GQD commonly used in clinical patients) and 8.64 g/kg (high dose, equivalent to the twice dosage of GQD commonly used in clinical patients).

2.2. Animals experiment

Six-week-old Sprague-Dawley rats (n = 86, males, weighing 180–220 g) were purchased from the Laboratory Animal Center of Shenyang Pharmaceutical University. The animals were raised in a dedicated SPF standard room with a temperature of 22 ± 2 °C, humidity of 40–60 %, and natural light and dark cycles from 7 am to 7 pm. All 86 rats were free to eat and drink for 7 days, and were deprived of water for 12 h before the experiment. The animal procedures were executed according to the SYPU Ethics Committee and carried out in line with the SYPU Guidelines for Animal Experimentation (SYPU-IACUC-S2022-07.28-201).

- I. After 7 days of adaptive feeding, 6 rats were randomly selected to collect blank plasma in the EDTA tube (orbital blood collection). Then GQD was given intragastric administration (8.64 g/kg) once a day for 7 days. Plasma samples were collected (orbital blood

Table 1

The detailed information of components in vitro and in vivo of Gegen Qinlian decoction (GQD).

Components in vitro of GQD							
No.	Identification	Formula	Found At Mass (m/z)	Ion adduction	Error/ppm	Rt (min)	Main product Ions (m/z, Da)
1	L-tryptophan	C ₁₁ H ₁₂ N ₂ O ₂	205.0962	[M + H] ⁺	-4.6	11.57	91.0546, 188.0697
2	Sucrose	C ₁₂ H ₂₂ O ₁₁	365.1046	[M + Na] ⁺	-2.2	4.00	185.0406, 203.0513
3	Daidzein	C ₁₅ H ₁₀ O ₄	255.0649	[M + H] ⁺	-1.1	39.22	91.0545, 137.0218, 199.0735, 227.0681, 237.0523
4	7,8,4'-Trihydroxyisoflavone	C ₁₅ H ₁₀ O ₅	271.05972	[M + H] ⁺	-1.4	45.89	169.0119, 253.0483
5	daidzein-4'-O-glucuronide	C ₂₁ H ₁₈ O ₁₀	431.09562	[M + H] ⁺	-3.8	40.32	255.0538, 269.0766
6	Puerarin	C ₂₁ H ₂₀ O ₉	417.11726	[M + H] ⁺	-1.8	25.70	267.0634, 297.0739, 351.0849, 381.0953, 399.1055
7	3'-Methoxypuerarin	C ₂₂ H ₂₂ O ₁₀	447.12684	[M + H] ⁺	-3.9	26.45	411.1020, 429.1116
8	Mirificin	C ₂₆ H ₂₈ O ₁₃	549.15779	[M + H] ⁺	-4.5	26.71	297.0735, 399.1048, 417.1150
9	Chrysin	C ₁₅ H ₁₀ O ₄	255.0649	[M + H] ⁺	-1.1	39.22	137.0218, 153.0684
10	Norwogonin	C ₁₅ H ₁₀ O ₅	270.0528	[M + H] ⁺	-1.0	36.93	123.0068, 169.0119, 253.0483
11	Baicalein	C ₁₅ H ₁₀ O ₅	271.0594	[M + H] ⁺	-0.7	31.31	169.0119, 253.0483
12	2',3,5,6',7-Pentahydroxyflavone	C ₁₅ H ₁₀ O ₇	302.0427	[M + H] ⁺	0.0	22.75	153.0158, 207.0275, 229.0476
13	quercetin	C ₁₅ H ₁₀ O ₇	303.0499	[M + H] ⁺	0.0	22.75	229.0925, 257.0797
14	Baicalein II	C ₁₆ H ₁₂ O ₆	301.07003	[M + H] ⁺	-2.1	45.87	286.0458, 301.0686
15	Dihydrooroxylin A	C ₁₆ H ₁₄ O ₅	287.0907	[M + H] ⁺	-2.4	41.31	168.0044, 183.0280, 287.0895
16	Scutellaria flavonoids I	C ₁₇ H ₁₄ O ₆	315.0855	[M + H] ⁺	-2.6	50.38	286.0784, 285.0748
17	5,7,2',5'-Tetrahydroxy-8,6'-dimethoxyflavone	C ₁₇ H ₁₄ O ₈	347.07529	[M + H] ⁺	-2.5	38.43	314.0404, 332.0511
18	Tenaxin I	C ₁₈ H ₁₆ O ₇	345.09596	[M + H] ⁺	-2.7	49.97	315.0483, 330.0719
19	Skullcapflavone II	C ₁₉ H ₁₈ O ₈	375.10594	[M + H] ⁺	-4.0	50.48	327.0474, 345.0571, 360.0815
20	Chrysin-7-O-glucuronide	C ₂₁ H ₁₈ O ₁₀	431.09562	[M + H] ⁺	-3.8	40.32	255.0685, 308.9824
21	Baicalin	C ₂₁ H ₁₈ O ₁₁	447.09054	[M + H] ⁺	-3.7	36.31	271.0583, 271.0379, 271.0594
22	Dihydrobaicalin	C ₂₁ H ₂₀ O ₁₁	449.10608	[M + H] ⁺	-3.9	36.68	131.0481, 169.0119, 273.0734
23	Chrysin-8-C-glucoside	C ₂₁ H ₂₀ O ₉	417.11726	[M + H] ⁺	-1.8	25.70	267.0740, 293.1011, 307.0919
24	Wogonoside	C ₂₂ H ₂₀ O ₁₁	461.10572	[M + H] ⁺	-4.6	41.54	285.0746, 270.0501, 285.0739
25	5,7,2'-trihydroxy-6-methoxyflavone 7-O-glucuronide	C ₂₂ H ₂₀ O ₁₂	477.10107	[M + H] ⁺	-3.5	39.11	286.0485, 301.0688
26	Isoscutellarein8-O-D-glucuronate	C ₂₄ H ₂₄ O ₁₂	505.13272	[M + H] ⁺	-2.6	35.35	127.0376, 137.0221, 257.0791
27	Tetraosane	C ₂₄ H ₅ O	310.0413	[M + H] ⁺	-0.1	23.86	71.0188
28	Amoenin A	C ₂₇ H ₃₄ O ₁₄	583.19985	[M + H] ⁺	-3.9	30.59	85.0281, 105.0697, 133.0634, 151.0365, 193.0488, 259.0946, 367.1162
29	Mullein glycoside	C ₂₉ H ₃₆ O ₁₅	625.21013	[M + H] ⁺	-4.1	32.47	163.0374, 273.0742, 607.1372
30	Keratocide D	C ₃₁ H ₄₀ O ₁₅	653.24124	[M + H] ⁺	-4.2	38.05	85.0304, 485.1510, 653.2460
31	p-hydroxybenzoic acid	C ₇ H ₆ O ₃	139.0387	[M + H] ⁺	-2.0	14.54	56.9658, 65.0382, 80.0493
32	2,3-dihydrobenzofuran	C ₈ H ₈ O	121.06443	[M + H] ⁺	-3.0	5.56	91.0557, 92.0242, 119.0349
33	2-methoxy-4-vinyl phenol	C ₉ H ₁₀ O ₂	151.07479	[M + H] ⁺	-3.8	6.64	77.0400, 137.0430
34	5-hydroxycoumarin	C ₉ H ₆ O ₃	163.03883	[M + H] ⁺	-0.9	19.14	51.0273, 135.0409, 163.0396
35	Transcafeic acid	C ₉ H ₈ O ₄	181.04958	[M + H] ⁺	0.2	38.77	153.0570, 181.0465
36	Ferulic acid	C ₁₀ H ₁₀ O ₄	195.06469	[M + H] ⁺	-2.5	24.90	145.0367, 177.0530
37	Noroxyhydrastinine	C ₁₀ H ₉ NO ₃	192.06562	[M + H] ⁺	0.5	31.41	134.0586, 149.0574
38	Cinnamic acid, 3,4-dimethoxy- (8CI)	C ₁₁ H ₁₂ O ₄	209.08102	[M + H] ⁺	0.9	35.17	69.9853, 129.9953, 148.9615
39	Corydaldine	C ₁₁ H ₁₃ NO ₃	208.09661	[M + H] ⁺	-1.0	30.96	77.0386, 91.0518, 105.0702
40	Moupinamide	C ₁₈ H ₁₉ NO ₄	314.13852	[M + H] ⁺	-0.5	40.84	117.0325, 121.0640, 145.0275, 177.0518
41	Coptisine	C ₁₉ H ₁₃ NO ₄	320.09133	[M + H] ⁺	-1.3	35.85	262.0833, 292.0926, 291.0888
42	Thalifendine	C ₁₉ H ₁₅ NO ₄	322.10664	[M + H] ⁺	-2.3	32.89	251.0888, 279.0838, 307.0808
43	Groenlandicine	C ₁₉ H ₁₅ NO ₄	322.10664	[M + H] ⁺	-2.3	32.89	279.0867, 307.0811
44	DeMethyleneberberine	C ₁₉ H ₁₇ NO ₄	324.12201	[M + H] ⁺	-3.2	32.44	280.0948, 294.0736, 309.0963
45	Berberine	C ₂₀ H ₁₇ NO ₄	336.12194	[M + H] ⁺	-3.2	39.68	278.0783, 292.0939, 306.0732, 320.0886
46	8-O-Berberine	C ₂₀ H ₁₇ NO ₅	352.11678	[M + H] ⁺	-3.3	33.30	308.0901, 322.0695, 336.0844
47	Jatrorrhizine	C ₂₀ H ₁₉ NO ₄	338.13732	[M + H] ⁺	-4.0	35.66	294.1100, 308.0900, 322.1048
48	(R)-Canadine	C ₂₀ H ₂₁ NO ₄	340.15343	[M + H] ⁺	-2.7	30.70	308.1263, 309.0980, 325.1284
49	Palmatine	C ₂₁ H ₂₁ NO ₄	352.15339	[M + H] ⁺	-2.7	39.40	294.1087, 309.1295, 336.1092, 337.1239
50	Limonin	C ₂₆ H ₃₀ O ₈	471.20235	[M + H] ⁺	2.1	19.85	274.1142, 471.1838
51	Acaciin	C ₂₈ H ₃₂ O ₁₄	593.18412	[M + H] ⁺	-4.0	30.69	365.1005, 575.1720, 593.1236
52	p-coumaric acid	C ₉ H ₈ O ₃	165.05429	[M + H] ⁺	-2.0	5.56	77.0393, 91.0537, 95.0498, 119.0476
53	Cis-Caffeic acid	C ₉ H ₈ O ₄	181.04958	[M + H] ⁺	0.2	38.77	147.0654, 163.0591
54	Glyzaglabrin	C ₁₆ H ₁₀ O ₆	299.05517	[M + H] ⁺	0.5	39.00	91.0540, 119.0511, 245.0380, 271.0580
55	HMO/isoformononetin	C ₁₆ H ₁₂ O ₄	269.08029	[M + H] ⁺	-2.0	47.71	237.0524, 254.0555
56	Vestitol	C ₁₆ H ₁₆ O ₄	273.11186	[M + H] ⁺	-1.0	19.85	137.0587, 149.0601
57	Glabranin	C ₂₀ H ₂₀ O ₄	325.14245	[M + H] ⁺	-3.0	52.59	123.0455, 189.0912, 325.1167
58	Sigmoidin-B	C ₂₀ H ₂₀ O ₆	357.1332	[M + H] ⁺	-0.2	51.01	127.0379, 147.0437, 175.0380, 357.1324
59	Vitexin	C ₂₁ H ₂₀ O ₁₀	433.11183	[M + H] ⁺	-2.5	21.44	283.0586, 313.0686, 337.0691
60	Astragaln	C ₂₁ H ₂₀ O ₁₁	449.10608	[M + H] ⁺	-3.9	36.68	273.0740, 274.0778, 449.1052, 450.1101
61	Gancaonin I	C ₂₁ H ₂₂ O ₅	355.15282	[M + H] ⁺	-3.3	52.46	271.0479, 299.0538
62	Liquiritin	C ₂₁ H ₂₂ O ₉	419.13211	[M + H] ⁺	-3.7	37.09	137.0226, 147.0431, 239.0680, 257.0790
63	Isoononin	C ₂₂ H ₂₂ O ₉	431.13225	[M + H] ⁺	-3.3	35.65	256.0621, 269.0794
64	Isoschaftoside	C ₂₆ H ₂₈ O ₁₄	565.15327	[M + H] ⁺	-3.4	29.40	447.1256, 565.1514, 566.1551
65	Kanzonol H	C ₂₆ H ₃₂ O ₅	425.23265	[M + H] ⁺	0.9	55.69	351.1212, 369.1290, 425.1926
66	Liquiritigenin	C ₁₅ H ₁₂ O ₄	257.08015	[M + H] ⁺	-2.7	31.98	91.0538, 119.0474, 137.0212
67	Isoliquiritigenin	C ₁₅ H ₁₂ O ₄	257.08015	[M + H] ⁺	-2.7	31.98	137.0218
68	Naringenin	C ₁₅ H ₁₂ O ₅	273.07556	[M + H] ⁺	-0.7	36.68	131.0477, 271.0497, 273.0755

(continued on next page)

Table 1 (continued)

Components in vitro of GQD							
No.	Identification	Formula	Found At Mass (m/z)	Ion adduction	Error/ppm	Rt (min)	Main product Ions (m/z, Da)
69	Formononetin	C ₁₆ H ₁₂ O ₄	269.08029	[M + H] ⁺	-2.0	47.71	197.0578, 237.0542, 254.0555
70	Medicarpin	C ₁₆ H ₁₄ O ₄	271.09577	[M + H] ⁺	-2.6	49.25	123.0435, 137.0529, 271.0981
71	12-Methyltetradecanoate	C ₁₆ H ₃₂ O ₂	257.24735	[M + H] ⁺	-0.6	61.07	69.0696, 81.0691
72	Odratin	C ₁₇ H ₁₄ O ₆	315.0855	[M + H] ⁺	-2.6	50.38	282.0493, 285.0366, 300.0589, 315.0821
73	Licoisoflavone B	C ₂₀ H ₁₆ O ₆	353.10112	[M + H] ⁺	-2.4	53.82	283.0598, 299.0545
74	Licoisoflavone	C ₂₀ H ₁₈ O ₆	355.11731	[M + H] ⁺	-0.9	52.15	121.0608, 149.0563, 353.1354
75	Corylifolinin	C ₂₀ H ₂₀ O ₄	325.14245	[M + H] ⁺	-3.0	52.59	149.0578, 171.0780, 325.1408
76	Glycyrrhizol	C ₂₁ H ₁₈ O ₆	367.11636	[M + H] ⁺	-3.4	53.19	283.0572, 311.0533, 309.0360, 339.1181
77	Isoliquiritin	C ₂₁ H ₂₂ O ₉	419.13211	[M + H] ⁺	-3.7	37.09	239.0680, 257.0790
78	Ononin	C ₂₂ H ₂₂ O ₉	431.13225	[M + H] ⁺	-3.3	35.65	256.0621, 269.0794, 270.0823
79	Glyasperins D	C ₂₂ H ₂₆ O ₅	371.18419	[M + H] ⁺	-3	54.48	235.1320, 303.1208, 315.1212
80	8-Methoxyformononetin	C ₂₃ H ₂₄ O ₁₀	461.14303	[M + H] ⁺	-2.6	29.86	253.0850, 281.0788, 299.0905
81	Glyasperin A	C ₂₅ H ₂₆ O ₆	423.17831	[M + H] ⁺	-4.5	55.97	311.0534, 367.1150
82	Glabrol	C ₂₅ H ₂₈ O ₄	393.20453	[M + H] ⁺	-3.8	55.21	205.0892, 321.1366
83	3-Hydroxyglabrol	C ₂₅ H ₂₈ O ₅	409.19911	[M + H] ⁺	-4.5	56.13	353.1361, 409.1983
84	Schaeffertoside	C ₂₆ H ₂₈ O ₁₄	565.15327	[M + H] ⁺	-3.4	29.40	397.0894, 415.0997, 433.1095
85	Glycyroside	C ₂₇ H ₃₀ O ₁₃	563.17391	[M + H] ⁺	-3.6	31.69	413.1213, 431.1316, 563.1726
86	Vicenin-2	C ₂₇ H ₃₀ O ₁₅	595.16363	[M + H] ⁺	-3.6	18.04	383.0697, 403.1316, 565.1693
87	Isoglycyrrhizinate and its isomers	C ₃₀ H ₄₄ O ₄	469.32961	[M + H] ⁺	-3.5	45.69	405.3087, 433.3086, 451.3179
88	beta-Glycyrrhetic acid	C ₃₀ H ₄₆ O ₄	471.34557	[M + H] ⁺	-2.8	47.70	317.2114, 407.3257, 471.3422
89	Ursolic acid	C ₃₀ H ₄₈ O ₃	457.3662	[M + H] ⁺	-3.1	48.02	123.1165, 375.1123, 457.2111
90	Glycyrrhizin	C ₄₂ H ₆₂ O ₁₆	823.40714	[M + H] ⁺	-4.8	47.70	453.3319, 454.3382, 471.3436, 647.3734
91	Licorice-saponin G2	C ₄₂ H ₆₂ O ₁₇	839.40276	[M + H] ⁺	-3.8	46.72	469.3271, 487.3378, 645.3599
92	(L)-alpha-Terpineol	C ₁₀ H ₁₈ O	155.14285	[M + H] ⁺	-1.2	49.32	81.0764, 95.0848, 109.0981, 127.1112
93	Licochalcone B	C ₁₆ H ₁₄ O ₅	287.0907	[M + H] ⁺	-2.4	41.31	168.0042, 183.0277
94	Chrysin	C ₁₅ H ₁₀ O ₄	253.04986	[M-H] ⁻	-3.1	34.34	254.0520, 253.0492
95	Daidzein	C ₁₅ H ₁₀ O ₄	253.04986	[M-H] ⁻	-3.1	34.34	91.0183, 133.0252, 209.0481, 224.0474
96	Genistein	C ₁₅ H ₁₀ O ₅	269.0452	[M-H] ⁻	-1.3	47.26	195.0387, 225.0443
97	3'-methoxydaidzein	C ₁₆ H ₁₂ O ₅	283.06031	[M-H] ⁻	-3.1	51.42	239.0337, 268.0369, 283.0611
98	puerol B	C ₁₈ H ₁₆ O ₅	311.09172	[M-H] ⁻	-2.5	37.69	93.0344, 119.0503, 267.1033
99	Genistin	C ₂₁ H ₂₀ O ₁₀	431.09809	[M-H] ⁻	-0.6	24.48	255.0666, 283.0610, 311.0560, 431.0991
100	Puerarin	C ₂₁ H ₂₀ O ₉	415.1027	[M-H] ⁻	-1.8	27.61	267.0666, 295.0618, 308.0643
101	3'-Methoxy Puerarin	C ₂₂ H ₂₂ O ₁₀	445.11334	[M-H] ⁻	-1.5	27.87	282.0518, 297.0763, 325.0706
102	Ononin	C ₂₂ H ₂₂ O ₉	429.11865	[M-H] ⁻	-1.1	33.09	266.0581, 281.0816, 309.0768
103	Genistein-8-C-xylosyl-(1-6)-glucoside	C ₂₆ H ₂₈ O ₁₄	563.1401	[M-H] ⁻	-0.9	30.66	283.0613, 311.0557, 563.1403
104	Baicalein	C ₁₅ H ₁₀ O ₅	269.0452	[M-H] ⁻	-1.3	47.26	223.0416, 241.0522, 269.0447
105	Chrysin-7-O-glucuronide	C ₂₁ H ₁₈ O ₁₀	429.08142	[M-H] ⁻	-3.0	42.53	209.0593, 252.2539, 253.0509
106	Baicalin	C ₂₁ H ₁₈ O ₁₁	445.07733	[M-H] ⁻	-0.7	38.20	159.0326, 269.0450, 275.0253
107	Darendroside B	C ₂₁ H ₃₂ O ₁₂	475.18183	[M-H] ⁻	-0.6	23.47	267.0665, 295.0617, 415.1032
108	Wogonoside	C ₂₂ H ₂₆ O ₁₁	459.09134	[M-H] ⁻	-4.2	43.53	175.0244, 268.0485, 283.0598, 459.0946
109	Chrysin 6-C-glucoside 8-C-arabinoside	C ₂₆ H ₂₈ O ₁₃	547.1453	[M-H] ⁻	-0.8	27.99	267.0656, 295.0604, 547.1451
110	Chrysin 7-O-Beta-Gentiobioside	C ₂₇ H ₃₀ O ₁₄	577.15679	[M-H] ⁻	0.9	21.04	294.0530, 429.1193, 457.1129
111	Martynoside	C ₃₁ H ₄₀ O ₁₅	651.229	[M-H] ⁻	-0.7	38.88	475.1835, 605.2107
112	Protocatechuic acid	C ₇ H ₆ O ₄	153.0191	[M-H] ⁻	-1.5	16.55	91.0200, 109.0301, 153.0200
113	3,4-Dimethoxycinnamic acid	C ₁₁ H ₁₂ O ₄	207.0660	[M-H] ⁻	-1.4	30.75	149.0554, 192.0361
114	3-Carboxy-4-hydroxy-phenoxy glucoside	C ₁₃ H ₁₆ O ₉	315.07188	[M-H] ⁻	-0.9	13.27	101.0288, 108.0221, 109.0305, 123.0441
115	Luteolin	C ₁₅ H ₁₀ O ₆	285.03954	[M-H] ⁻	-3.2	46.53	151.0045, 175.0388, 199.0410, 267.0295
116	Rosmarinic acid	C ₁₈ H ₁₆ O ₈	359.07592	[M-H] ⁻	-3.7	50.29	344.0530, 359.0763
117	Pinoretinol glucoside	C ₂₆ H ₃₂ O ₁₁	519.18673	[M-H] ⁻	-0.9	33.21	151.0375, 309.0671
118	(+)-lariciresinol glucoside	C ₂₆ H ₃₄ O ₁₁	521.20243	[M-H] ⁻	-0.8	30.78	299.1417, 329.1391
119	Malic acid	C ₄ H ₆ O ₅	133.01417	[M-H] ⁻	-0.6	4.63	71.0287, 115.0033, 133.0121
120	Danshensu	C ₉ H ₁₀ O ₅	197.04533	[M-H] ⁻	-1.1	12.29	123.0454, 135.0450, 179.0281, 179.040, 197.0502
121	Isoliquiritigenin	C ₁₅ H ₁₂ O ₄	255.06548	[M-H] ⁻	-3.2	45.23	91.0216, 119.0514, 135.0102
122	Carthamidin	C ₁₆ H ₁₂ O ₆	299.05521	[M-H] ⁻	-3.0	47.07	284.0325, 299.0554
123	Liquiritin	C ₂₁ H ₂₂ O ₉	417.11814	[M-H] ⁻	-2.3	33.64	91.0203, 119.0506, 135.0088, 255.0657
124	Isoliquiritin	C ₂₁ H ₂₂ O ₉	417.11814	[M-H] ⁻	-2.3	33.64	119.0505, 135.0088, 255.0665
125	Narcissoside	C ₂₈ H ₃₂ O ₁₆	623.16207	[M-H] ⁻	0.5	24.33	415.1018, 416.1060, 623.1650
126	Glycyrrhizin	C ₄₂ H ₆₂ O ₁₆	821.39572	[M-H] ⁻	-1.0	47.53	351.0554, 822.3965
127	Darendoside A	C ₁₉ H ₂₈ O ₁₁	431.15585	[M-H] ⁻	-0.1	20.80	191.0572, 233.0653, 311.0557
Components in vivo of GQD							
No.	Identification	Formula	Found At Mass (m/z)	Ion adduction	Error/ppm	Rt (min)	Main product Ions (m/z, Da)
1	Daidzein	C ₁₅ H ₁₀ O ₄	255.06507	[M + H] ⁺	-0.5	39.86	91.0548, 137.0245, 199.0747, 227.0704, 237.0556
2	7,8,4'-Trihydroxyisoflavone	C ₁₅ H ₁₀ O ₅	271.06021	[M + H] ⁺	0.4	45.98	215.0764, 243.0605
3	Puerarin	C ₂₁ H ₂₀ O ₉	417.11698	[M + H] ⁺	-2.5	26.11	267.0645, 297.0745, 351.0846, 381.0953, 399.1050
4	3'-Methoxypuerarin	C ₂₂ H ₂₂ O ₁₀	447.12707	[M + H] ⁺	-3.4	26.71	297.0771, 411.1061, 429.1152
5	Mirificin	C ₂₆ H ₂₈ O ₁₃	549.15845	[M + H] ⁺	-3.3	26.93	297.0758, 399.1067, 417.1177
6	Chrysin	C ₁₅ H ₁₀ O ₄	255.06507	[M + H] ⁺	-0.5	39.86	152.0614, 227.0704
7	Dihydrooroxylin A	C ₁₆ H ₁₄ O ₅	287.09119	[M + H] ⁺	-0.7	42.03	69.0743, 168.0046
8	Skullcapflavone II	C ₁₉ H ₁₈ O ₈	375.10734	[M + H] ⁺	-0.3	50.73	227.0544, 327.0400, 345.0609
9	Baicalin	C ₂₁ H ₁₈ O ₁₁	447.09137	[M + H] ⁺	-1.8	32.73	271.0596
10	Chrysin-8-C-glucoside	C ₂₁ H ₂₀ O ₉	417.11698	[M + H] ⁺	-2.5	26.11	267.0645, 297.0745, 417.1166

(continued on next page)

Table 1 (continued)

Components in vitro of GQD		Formula	Found At Mass (m/z)	Ion adduction	Error/ppm	Rt (min)	Main product Ions (m/z, Da)
No.	Identification						
11	Wogonoside	C ₂₂ H ₂₀ O ₁₁	461.10681	[M + H] ⁺	-2.2	42.09	270.0516, 285.0752
12	Coptisine	C ₁₉ H ₁₃ NO ₄	320.09171	[M + H] ⁺	-0.1	37.04	262.0860, 277.0731, 292.0963
13	Thalifendine	C ₁₉ H ₁₅ NO ₄	322.10701	[M + H] ⁺	-1.2	33.29	250.0866, 279.0906
14	Groenlandicine	C ₁₉ H ₁₅ NO ₄	322.10701	[M + H] ⁺	-1.2	33.29	207.0833
15	DeMethyleneberberine	C ₁₉ H ₁₇ NO ₄	324.12271	[M + H] ⁺	-1.0	32.72	280.0961, 309.0979
16	Berberine	C ₂₀ H ₁₇ NO ₄	336.1227	[M + H] ⁺	-1.0	41.49	292.0973, 306.0769, 320.0915
17	Jatrorrhizine	C ₂₀ H ₁₉ NO ₄	338.13847	[M + H] ⁺	-0.6	35.97	279.0884, 294.1113, 323.1140
18	Palmatine	C ₂₁ H ₂₁ NO ₄	352.15399	[M + H] ⁺	-1.0	40.89	308.1276, 336.1225, 337.1306
19	p-coumaric acid	C ₉ H ₈ O ₃	165.05409	[M + H] ⁺	-3.2	5.58	91.0545, 119.0495, 123.0440, 147.0399
20	Astragalin	C ₂₁ H ₂₀ O ₁₁	449.1061	[M + H] ⁺	-3.9	34.51	273.0721, 449.1996
21	Isooononin	C ₂₂ H ₂₂ O ₉	431.13329	[M + H] ⁺	-0.9	35.96	269.0805, 431.1117
22	Liquiritigenin	C ₁₅ H ₁₂ O ₄	257.08059	[M + H] ⁺	-1.0	32.72	91.0568, 119.0498, 137.0228
23	Isoliquiritigenin	C ₁₅ H ₁₂ O ₄	257.08059	[M + H] ⁺	-1.0	32.72	137.0228, 147.0413
24	Ononin	C ₂₂ H ₂₂ O ₉	431.13329	[M + H] ⁺	-0.9	35.96	213.0971, 254.0557, 269.0805, 431.1117
25	Glyasperin A	C ₂₅ H ₂₆ O ₆	423.18008	[M + H] ⁺	-0.3	58.82	327.2220, 367.2001
26	Glycyrrhizin	C ₄₂ H ₆₂ O ₁₆	823.40792	[M + H] ⁺	-3.8	47.72	453.3350, 471.3325, 647.3756
27	Licorice-saponin G2	C ₄₂ H ₆₂ O ₁₇	839.40909	[M + H] ⁺	3.7	47.32	839.4986
28	(L)-alpha-Terpineol	C ₁₀ H ₁₈ O	155.1427	[M + H] ⁺	-1.2	49.64	156.7057, 157.0821
29	Licochalcone B	C ₁₆ H ₁₄ O ₅	287.0911	[M + H] ⁺	-0.7	41.03	69.0743, 168.0046
30	Genistein	C ₁₅ H ₁₀ O ₅	269.0454	[M-H] ⁻	-0.5	47.68	63.0251, 157.0377, 224.0498
31	3'-methoxydaidzein	C ₁₆ H ₁₂ O ₅	283.06096	[M-H] ⁻	-0.8	51.48	239.0340, 268.0383, 283.0592
32	Puerarin	C ₂₁ H ₂₀ O ₉	415.10221	[M-H] ⁻	-3.0	27.39	267.0651, 295.0590, 307.0558
33	3'-Methoxy Puerarin	C ₂₂ H ₂₂ O ₁₀	445.11259	[M-H] ⁻	-3.2	27.71	297.0774, 325.0689, 430.0994
34	Baicalin	C ₂₁ H ₁₈ O ₁₁	445.07668	[M-H] ⁻	-2.2	34.35	85.0298, 113.0247, 269.0440
35	Wogonoside	C ₂₂ H ₂₀ O ₁₁	459.09206	[M-H] ⁻	-2.7	43.68	175.0256, 268.0366, 283.0605
36	Chrysin 6-C-glucoside 8-C-arabinoside	C ₂₆ H ₂₈ O ₁₃	547.14423	[M-H] ⁻	-2.7	27.82	277.0519, 295.0606, 325.0709
37	Chrysin 7-O-Beta-Gentiobioside	C ₂₇ H ₃₀ O ₁₄	577.15547	[M-H] ⁻	-1.4	20.62	457.0922, 508.9563
38	Isoliquiritin	C ₂₁ H ₂₂ O ₉	417.11796	[M-H] ⁻	-2.7	35.98	119.0520, 135.0450
39	Glycyrrhizin	C ₄₂ H ₆₂ O ₁₆	821.39558	[M-H] ⁻	-1.1	47.64	351.0540, 822.4001
40	Baicalein	C ₁₅ H ₁₀ O ₅	269.0454	[M-H] ⁻	-0.5	47.68	63.0251, 169.0649, 224.0498, 268.7776

collection) at 0.5 h, 1 h, 2 h and 4 h after the last administration for subsequent analysis.

- II. The remaining rats were randomly divided into 10 groups (n = 8): (1) control; (2) UC (after anesthesia with 30 mg/kg pentobarbital sodium, rats were given enema by injecting TNBS (100 mg/kg)-50 % ethanol mixture into the anuses of the rats); (3) UL (low-dose GQD to treat UC); (4) UH (high-dose GQD to treat UC); (5) CRC (Intraperitoneal injection of 30 mg/kg DMH once a week for 13 weeks, continued to induce cancer based on UC); (6) RL (low-dose GQD for the treatment of CRC); (7) RH (high-dose GQD for the treatment of CRC); (8) XELOX (4 mg/kg Oxaliplatin intraperitoneal injection once a week and 150 mg/kg capecitabine intragastric injection once a day for CRC rats); (9) RXL (low-dose GQD combined with XELOX for the treatment of CRC); (10) RXH (high-dose GQD combined with XELOX for the treatment of CRC).

After 12 h of fasting, rats were given TNBS (100 mg/kg)-50 % ethanol enema to induce UC, UL and UH rats were given GQD intragastric administration for 7 days, and daily weight was registered. On the 7th day after modeling, the disease activity index (DAI) score was recorded. For specific scoring criteria, please refer to Table S1.

After the last dose, orbital venous blood of each group was collected in coagulant tubes and centrifuged at 4000 rpm for 10 min to collect serum samples. After the colon contents were collected, the colon was cleaned with physiological saline. Then, the colonic mucosal damage index (CMDI) was scored by observing the gross morphology of colon tissues. The scoring criteria and results were shown in Table S1. Part of colon tissues were clipped for Hematoxylin-eosin (HE) staining, and the remaining were immediately frozen at -80 °C.

Then, CRC, RL, RH, XELOX, RXL and RXH groups were given DMH (30 mg/kg) by intraperitoneal injection once a week for 13 weeks to continue to induce CRC. The rats in RL, RH, RXL and RXH groups were given GQD, while the rats in XELOX group were given the XELOX continuously for 6 weeks. Sample collection methods were the same as above.

2.3. HE staining

Colon tissues were fixed with paraformaldehyde (4 %). More than 24 h later, paraffin was adopted for embedding and section. After dewaxing, hydration and HE staining were carried out successively. Ultimately, the slices were observed under a 200-fold microscope and photographed.

2.4. Component identification experiment

- I. Preparation of GQD for the analysis of vitro components: GQD was prepared according to the prescription ratio (8:3:3:2), and the filtrate was concentrated at 50 °C to the relative density of 1.05. A certain volume was taken and diluted with an appropriate amount of methanol, which was equivalent to 0.1 g crude drug per 1 mL. The liquid was filtered by 0.22 μm for instrumental use.
- II. Preparation of plasma samples for the analysis of components in vivo: 1 mL plasma sample mixed with 3 mL methanol, then vortexed for 3 min and centrifugated at 12,000 rpm (5 min, 4 °C). The supernatant was dry by placed under nitrogen flow and then added with 50 μL methanol, followed by vortexed for 3 min, ultrasound and centrifugated (5 min, 12,000 rpm, 4 °C). After that, the supernatant was separated for instrumental analysis.

The chromatographic and mass spectrum conditions were shown in Table S2-3. Then, the chemical composition of GQD were analyzed and identified using PeakView 1.2.1 (SCIEX, Framingham, MA, USA) software.

2.5. Network pharmacology analysis

The target of the components in plasma was predicted based on SwissTargetPrediction website (<https://www.swisstargetprediction.ch>). To obtain the key targets of components in plasma, SMILES strings of these components in vivo were entered into SwissTargetPrediction

(<https://www.swisstargetprediction.ch>), from which possible targets for these compounds were returned based on predicted probability ranking order. Meanwhile, the genes of UC and CRC were obtained on Therapeutic Target Database (TTD, <https://db.idrblab.net/ttd/>) and GeneCards (<https://www.genecards.org>), with “Ulcerative colitis” and “Colorectal cancer” as keywords. Venny (<https://www.liuxiaoyuuan.cn/>) website was used to compare the differential genes of diseases and the targets of the components of GQD in plasma, and the intersection targets were selected. A protein–protein interaction (PPI) network was drawn through String database (<https://cn.string-db.org/>). Finally, the “herb-component-target” network was constructed by Cytoscape 3.10.0 (UC, San Diego, La Jolla, CA, USA).

2.6. Elisa assay

The expression levels of VEGF, SOD, TNF- α , IL-1 β , MDA, IL-6 and IL-10 in colon and serum were quantitatively determined by ELISA kit according to the product description. First, 50 μ L standard products in kit with different concentrations and 50 μ L samples to be tested were added in each hole, and nothing is added to the blank hole. Next, each standard and sample holes were added with 100 μ L of HRP labeled

detection antibody and incubated in a 37 °C incubator for 60 min, and then washed with washing buffer for 3 times. 50 μ L substrate A and 50 μ L B were added to each hole. After incubation at 37 °C for 15 min, 50 μ L termination solution was added to each hole successively. Finally, OD value of each hole was measured at 450 nm by enzyme-labeled instrument.

2.7. Flow cytometry detected of T lymphocytes (CD4⁺ and CD8⁺)

First, 0.5 mL blood was diluted to 3 mL and placed on 3 mL lymphocyte separation solution, and centrifuge at 400 g (20 min). The lymphocyte layer was cleaned with cleaning solution centrifuged for 10 min (250 g). Next, the precipitation was mixed with RBC lysate (3 mL) and incubated on ice (10 min), followed by terminated with PBS. The underlying cells were retained after centrifugation. PBS was used for suspending the cells, and then 0.5 μ g FITC-CD3⁺, 0.25 μ g APC-CD4⁺ and 0.25 μ g PE-CD8⁺ were added and stained at 4 °C for 1 h away from light. 500 μ L PBS was added and centrifuged 250 g for 10 min for cleaning. The underlying cells were re-suspended with PBS and transferred to the flow tube. Flow cytometry was adopted for detecting and calculating the proportions of CD4⁺ and CD8⁺ T lymphocytes.

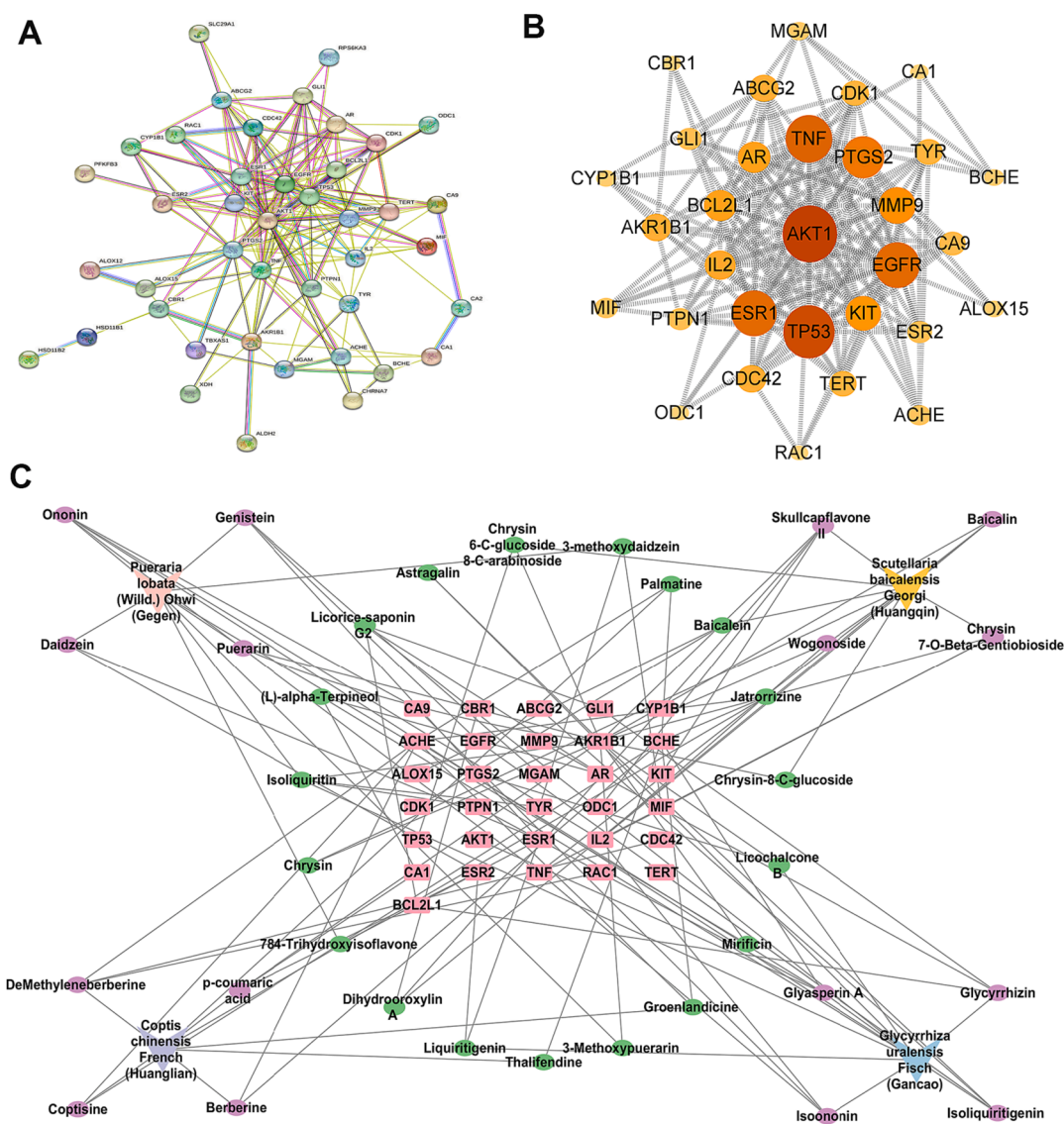


Fig. 1. Prediction results of network pharmacology study. PPI diagram network (A); Network diagram of 31 key targets (B); “Herb-component-target” multivariate network (C).

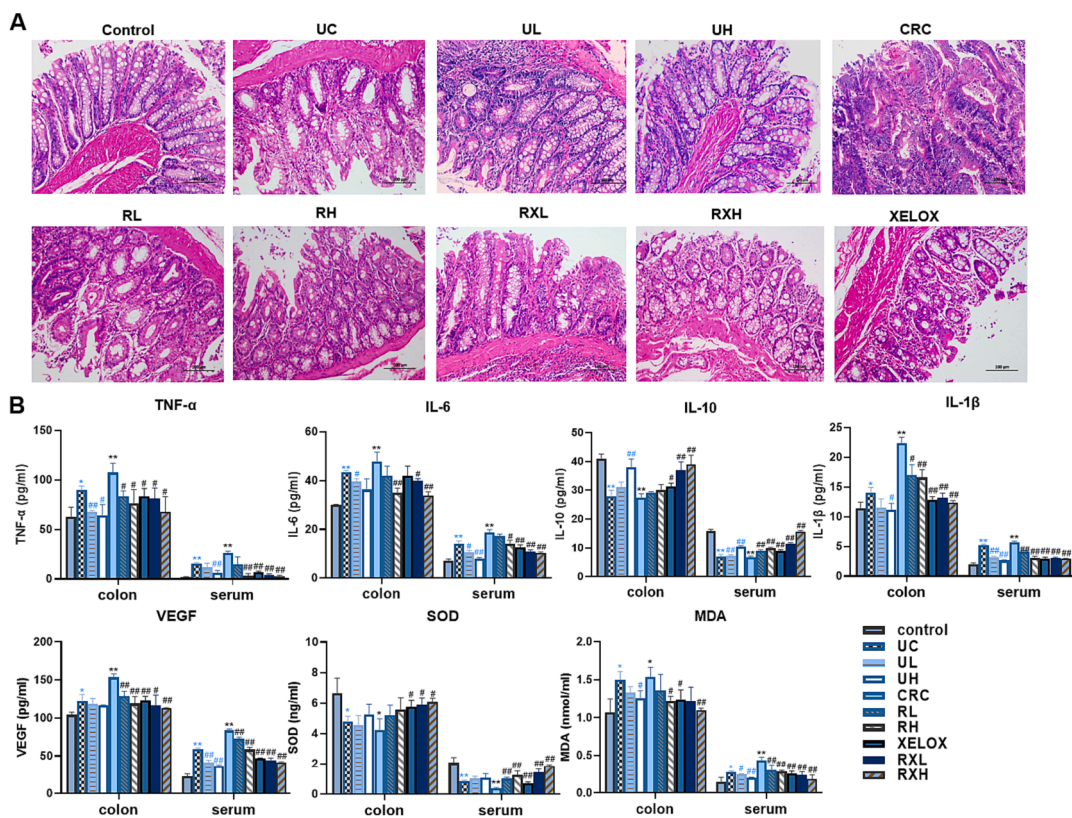


Fig. 2. H&E staining results of colon tissues (200 \times magnification) (A); Bar chart of ELISA kit results for inflammatory factors, tumor factors and antioxidant indicators (B). Values shown are means \pm SD. * $p < 0.05$, ** $p < 0.01$ UC vs Control group; * $p < 0.05$, ** $p < 0.01$ CRC vs Control group; # $p < 0.05$, ## $p < 0.01$ vs UC group; # $p < 0.05$, ## $p < 0.01$ vs CRC group.

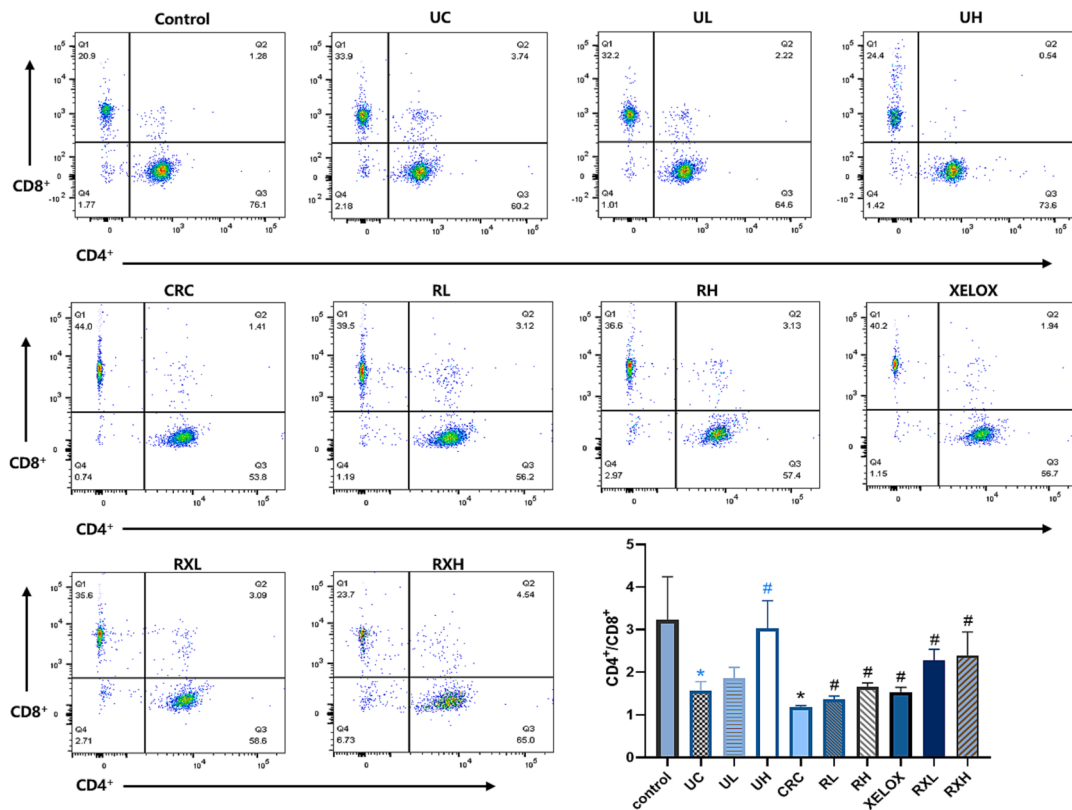


Fig. 3. Flow cytometric analysis of CD4⁺ and CD8⁺ cells in each group of rats. * $p < 0.05$ UC vs control group; * $p < 0.05$ CRC vs Control group; # $p < 0.05$ vs UC group; # $p < 0.05$ vs CRC group.

2.8. Intestinal microflora detection and data processing methods

DNA was extracted from every 0.1 g of frozen colon contents and genomic DNA integrity (including purity and concentration) was examined by 1 % agar-gel electrophoresis. The PCR amplification system was 20 μ L, and the V3-V4 region was amplified using the universal primers 338F (5'-ACTCTACGGGAGGAGCAG-3') and 806R (5'-GGACTACHVGGGTWTCTAAT-3'). Next, the products were identified, purified and quantified. Sequencing was then performed on the Illumina MiSeq PE250 system. Trimmomatic (v0.33) was used to filter the sequenced Raw Reads. And cutadapt 1.9.1 software was used to identify and remove primer sequences, then Clean Reads without primer sequences were obtained. After a series of preprocessing, the original data were obtained with high quality sequences, and then OUT clustering and species annotation were carried out. According to the annotation results, distribution histogram of the top 10 community in abundance at different levels were drawn by QIIME2 (<https://qiime2.org>). In addition, linear discriminant analysis (LDA, <https://huttenhower.sph.harvard.edu/lefse/>) was used to estimate the influence of microflora abundance on the difference effect. Finally, the significance analysis of inter-group differences (Metastats, <https://metastats.cbc.umd.edu/>) was used to measure the differences in microflora abundance composition in disease group, control group and drug intervention groups, and to find biomarkers with statistical differences.

2.9. Metabolomics detection and data processing methods

1 mL of physiological saline and 100 mg of colon tissue were combined and homogenized for 3 min. Then, 500 μ L of homogenate

supernatant was measured and added with 10 μ L internal standard solution (10 μ g/mL of L-2-Chlorophenylalanine and heptadecanoic acid) and 1.5 mL methanol. The mixture was vortexed for 3 min before being centrifuged (12,000 rpm for 10 min at 4 $^{\circ}$ C). The residue dried by nitrogen was then redissolved with 100 μ L methanol, swirled for 3 min, ultrasonically for 3 min, then centrifuged (5 min, 12,000 rpm). The supernatant was collected for instrument analysis and detailed chromatographic and mass spectrum conditions were presented in the Table S4-5.

The original data was imported into XCMS (<https://xcmsonline.scripps.edu/>) platform for peak identification, peak matching and other processing. Principal component analysis (PCA) was performed on the processed data using SIMCA-P 14.0 (Umetrics, Malmo, Sweden), followed by orthogonal partial least squares discriminant analysis (OPLS-DA) and 200 permutation tests. Subsequently, a combination of multiple indicators was used to determine the differential metabolites. Subsequently, based on the precise mass/charge ratio and MS/MS information provided by HPLC-Q-TOF-MS/MS, the differential metabolites were identified using HMDB (<https://hmdb.ca/>), MetDNA (<https://metdna.zhulab.cn/>) and Mzcloud (<https://www.mzcloud.org>) databases. Then, MetaboAnalyst (<https://www.metabo-analyst.ca/>) platform was used for the analysis of KEGG pathway enrichment of differential metabolites. In addition, Spearman analysis between differential microflora and metabolites were conducted and visualized by heatmap. Finally, Met-scape was used to obtain compound-reaction-enzyme-gene interaction networks to realize integrated analysis of network pharmacology and metabolomics.

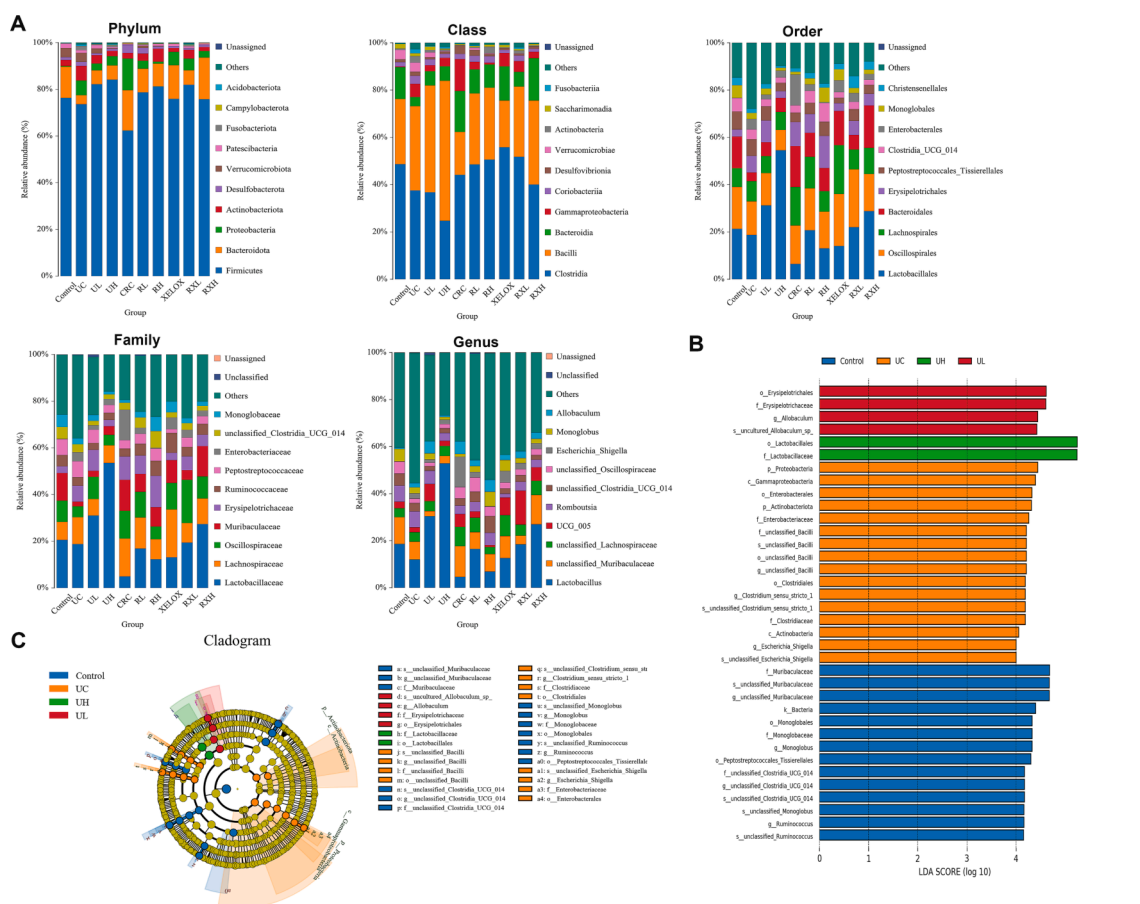


Fig. 4. Distribution histogram of the top 10 community in abundance at the level of phylum, class, order, family and genus (A); Distribution histogram based on LDA of dominant microorganisms in the control, UC, UL, UH groups (B); Cladogram of dominant microorganisms in the control, UC, UL, UH groups (C).

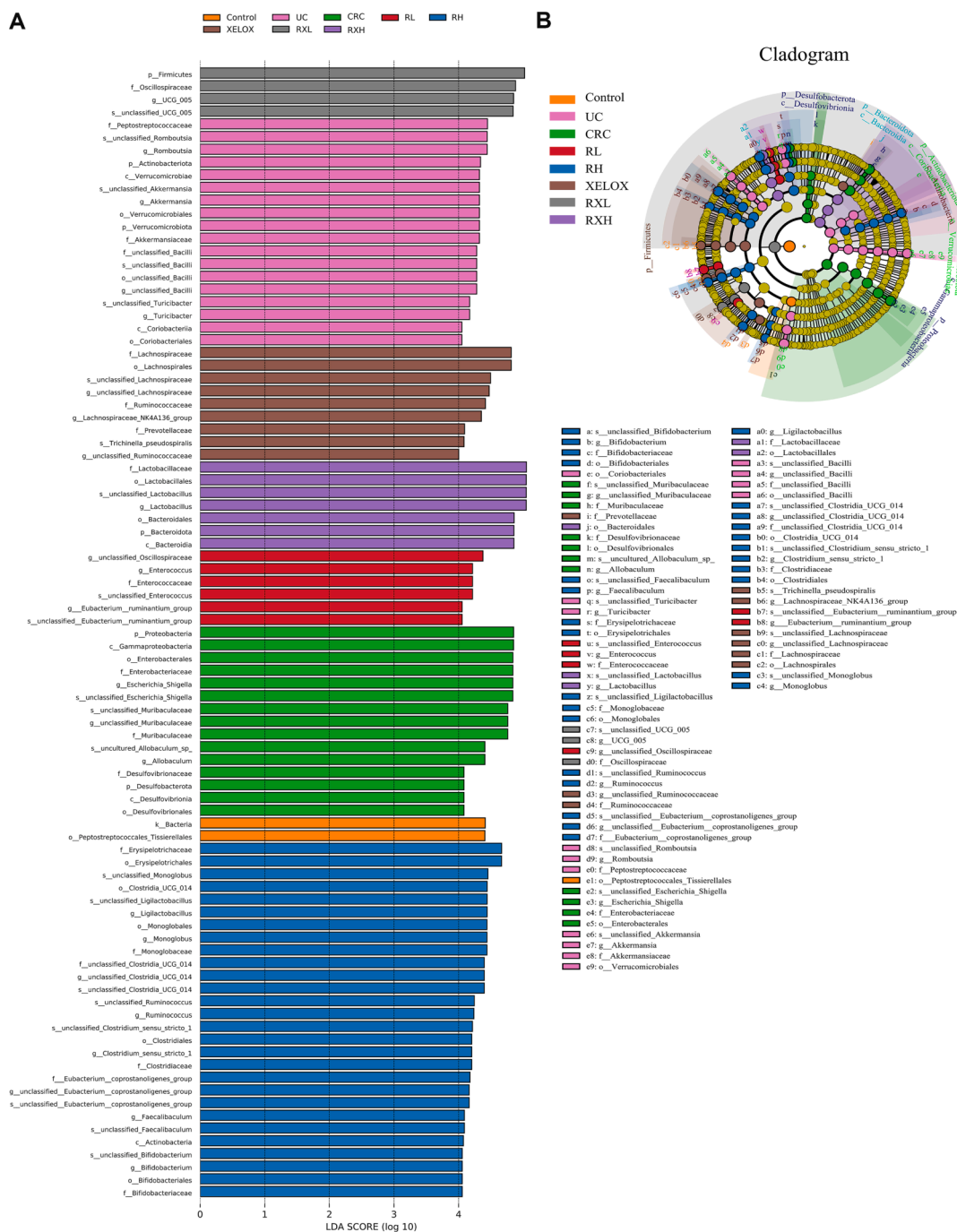


Fig. 5. Distribution histogram based on LDA of dominant microorganisms in different groups (A); Cladogram of dominant microorganisms in different groups (B).

2.10. Western blot analysis of crucial target proteins

Using the Pierce™BCA Protein Quantification Kit (Thermo, San Jose, CA, USA), the total proteins in the colon tissues were measured. Colon samples were diluted and added to 5 × protein loading buffer (Epizyme, Shanghai, China) to achieve a final protein concentration of 4 g/L (the volume ratio of samples to loading buffer was 4:1). For further examination, all samples were then denatured for 10 min (100 °C). After adding 2.5 μL of marker (Fisher, San Jose, CA, USA), 40 μg samples were added, sodium dodecyl sulfate–polyacrylamide gel electrophoresis from 60 V to 110 V were carried out. Then, the electric transfer was performed at 240 mA. Membranes were then blocked for 30 min using blocking solution (Genefist, Oxfordshire, UK), and then eluted for 3 times with TBST (Solarbio, Beijing, China). Next, the bands were incubated in

ALOX15 (1:1000), CYP1B1 (1:5000), PTGS2 (1:1000) and β-actin (colon loading control, 1:1000) primary antibodies overnight at 4 °C. Then, the protein bands were re-elution of TBST for 3 times, followed by incubated with 1:5000 secondary antibodies (bs-40295G-HRP; Biomass) away from light for 1 h. After coated with ECL developer solution evenly (US Everbright, Suzhou, China), the target bands were visualized by Tanon 5200 Multi fully automated chemiluminescence image analysis system (Tanon, Shanghai, China). Finally, ImageJ (Rawak Software Inc., Stuttgart, Germany) software was utilized for the purpose of quantification.

2.11. Molecular docking

The protein files of ALOX15 (PDB: 2p0m), CYP1B1 (PDB: 3 pm0) and

Table 2

The detailed information of potential biomarker detected in the ulcerative colitis (UC) group and colorectal cancer (CRC) group.

No.	t(R)	ESI mode	m/z	Identification	Fomular	FC1	VIP1	FC2	VIP2	Change trend UC/Con.	CRC/Con.	CRC/UC
1	3.3	+	130.0855	Pipelic acid	C ₆ H ₁₁ NO ₂	0.42	1.17			↑		
2	7.2	+	134.0593	Indoxyl	C ₈ H ₇ NO			0.35	1.07		↑	
3	7.0	+	243.1005	Equol	C ₁₅ H ₁₄ O ₃	0.02	2.58			↑		
4	3.0	+	258.1090	Glycerophosphocholine	C ₈ H ₂₀ NO ₆ P	0.30	1.18			↑		
5	9.2	+	300.2883	Sphingosine	C ₁₈ H ₃₇ NO ₂	0.23	1.53	0.24	1.21	↑	↑	↓
6	12.3	+	301.2149	(6Z,9Z,12Z)-Octadecatrienoic acid	C ₁₈ H ₃₀ O ₂	0.35	1.28			↑		
7	12.9	+	303.2306	9-cis,11-trans-Octadecadienoate	C ₁₈ H ₃₂ O ₂	0.40	1.20			↑		
8	10.7	+	375.2868	Murideoxycholic acid	C ₂₄ H ₄₀ O ₄	0.48	1.13	0.13	1.49	↑	↑	↑
9	11.3	+	375.2871	3-Oxo-5beta-cholanate	C ₂₄ H ₃₈ O ₃	0.26	1.55	0.07	1.68	↑	↑	↑
10	9.6	+	380.2539	S1P(d18:1)	C ₁₈ H ₃₈ NO ₅ P			4.12	1.20		↓	
11	9.9	+	389.2660	7-Oxodeoxycholate	C ₂₄ H ₃₈ O ₅			0.06	1.75		↑	
12	10.8	+	391.2816	3alpha,12alpha-Dihydroxy-5beta-chole-6-enoate	C ₂₄ H ₃₈ O ₄	0.34	1.32	0.01	2.23	↑	↑	↑
13	10.1	+	393.2978	Chenodeoxycholic acid	C ₂₄ H ₄₀ O ₄			0.34	1.04		↑	
14	11.4	+	393.2984	Hyodeoxycholic acid	C ₂₄ H ₄₀ O ₄			0.11	1.56		↑	
15	9.0	+	407.2765	7-Ketodeoxycholic acid	C ₂₄ H ₃₈ O ₅	0.33	1.46	0.01	2.32	↑	↑	↑
16	8.8	+	409.2911	omega-Muricholic acid	C ₂₄ H ₄₀ O ₅	0.48	1.16	0.11	1.55	↑	↑	↑
17	9.5	+	409.2918	Ursodeoxycholic acid	C ₂₄ H ₄₀ O ₅	0.27	1.55	0.16	1.44	↑	↑	↑
18	8.6	+	450.3178	Glycodeoxycholic acid	C ₂₆ H ₄₃ NO ₅	0.21	1.58	0.32	1.12	↑	↑	↑
19	9.8	+	450.3179	Glycochenodeoxycholic acid	C ₂₆ H ₄₃ NO ₅	0.12	1.92			↑		
20	8.3	+	466.3130	Glycocholic acid	C ₂₆ H ₄₃ NO ₆	0.13	1.85			↑		
21	10.7	+	482.3208	LPC(15:0)	C ₂₃ H ₄₈ NO ₇ P	0.33	1.33					
22	8.5	+	484.3046	Taurolithocholic acid	C ₂₆ H ₄₅ NO ₅ S			0.34	1.04		↑	
23	10.0	+	489.2569	Cholic acid 7-sulfate	C ₂₄ H ₄₀ O ₆ S			0.02	2.04		↑	
24	7.8	+	498.2848	Taurohyocholate	C ₂₆ H ₄₅ NO ₇ S			0.04	1.83		↑	
25	8.1	+	500.2995	Taurodeoxycholic acid	C ₂₆ H ₄₅ NO ₆ S	0.23	1.69	0.50	1.07	↑	↑	↓
26	12.1	+	510.3520	LPC(17:0/0:0)	C ₂₅ H ₅₂ NO ₇ P	0.35	1.29			↑		
27	7.5	+	516.2942	Tauro-gamma-muricholic acid	C ₂₆ H ₄₅ NO ₇ S	0.42	1.09			↑		
28	8.2	+	516.2947	Taurocholic acid	C ₂₆ H ₄₅ NO ₇ S	0.39	1.26			↑		
29	8.1	+	569.3261	Chenodeoxycholic acid 3-glucuronide	C ₃₀ H ₄₈ O ₁₀			0.00	2.68		↑	
30	5.1	-	117.0200	Succinate	C ₄ H ₆ O ₄			2.28	1.02		↓	
31	2.9	-	124.0080	Taurine	C ₂ H ₇ NO ₃ S			2.75	1.12		↓	
32	3.1	-	130.0627	Creatine	C ₄ H ₉ N ₃ O ₂			2.73	1.16		↓	
33	6.6	-	158.0824	Isovalerylglycine	C ₇ H ₁₃ NO ₃	23.16	1.96	6.81	1.64	↓	↓	↑
34	7.2	-	172.9914	Phenylsulfate	C ₆ H ₆ O ₄ S	5.58	1.43	3.12	1.23	↓	↓	↑
35	3.3	-	173.0934	N-Acetylmuricholic acid	C ₇ H ₁₄ N ₂ O ₃	0.15	1.48			↑		
36	6.6	-	181.0507	Hydroxyphenyllactic acid	C ₉ H ₁₀ O ₄			0.22	1.37		↑	
37	7.5	-	187.0975	Azelaic acid	C ₉ H ₁₆ O ₄			0.24	1.37		↑	
38	4.5	-	191.0197	Citric acid	C ₆ H ₈ O ₇	0.21	1.29	0.19	1.42	↑	↑	↑
39	3.0	-	195.0511	Gluconic acid	C ₆ H ₁₂ O ₇			0.28	1.26		↑	
40	7.2	-	206.0822	N-Acetylphenylalanine	C ₁₁ H ₁₃ NO ₃	6.21	1.47			↓		
41	6.9	-	216.9809	5-Sulfosalicylate	C ₇ H ₆ O ₆ S			0.07	1.82		↑	
42	7.3	-	233.0426	S-(4-Methylthiobutylthiohydroximoyl)-L-cysteine	C ₈ H ₁₆ N ₂ O ₃ S ₂	0.35	1.09	0.15	1.60	↑	↑	↑
43	15.1	-	253.2167	cis-9-Palmitoleic acid	C ₁₆ H ₃₀ O ₂	0.23	1.26			↑		
44	16.1	-	255.2323	Palmitic acid	C ₁₆ H ₃₂ O ₂	0.37	1.03			↑		
45	14.2	-	271.2271	2-Hydroxypalmitic acid	C ₁₆ H ₃₂ O ₃			2.95	1.15		↓	
46	14.9	-	277.2165	alpha-Linolenic acid	C ₁₈ H ₃₀ O ₂	0.25	1.24	0.17	1.55	↑	↑	↑
47	15.5	-	279.2320	Linoleic acid	C ₁₈ H ₃₂ O ₂	0.36	1.07	0.26	1.32	↑	↑	↑
48	16.4	-	281.2477	Oleic acid	C ₁₈ H ₃₄ O ₂	0.37	1.05	0.29	1.28	↑	↑	↑
49	17.4	-	283.2634	Stearic acid	C ₁₈ H ₃₆ O ₂	0.25	1.14			↑		
50	12.6	-	295.2268	13(S)-HODE	C ₁₈ H ₃₂ O ₃	0.18	1.41	0.13	1.63	↑	↑	↑
51	17.8	-	297.2426	9-Oxooctadecanoic acid	C ₁₈ H ₃₄ O ₃	0.11	1.54			↑		
52	15.7	-	299.2584	2-Hydroxystearic acid	C ₁₈ H ₃₆ O ₃	0.22	1.28			↑		
53	16.0	-	305.2476	cis-8,11,14-Eicosatrienoic acid	C ₂₀ H ₃₄ O ₂	0.16	1.44	0.17	1.54	↑	↑	↓
54	16.7	-	307.2632	cis-11,14-Eicosadienoic acid	C ₂₀ H ₃₆ O ₂	0.26	1.22	0.41	1.06	↑	↑	↓
55	17.6	-	309.2788	trans-11-Eicosenoic acid	C ₂₀ H ₃₈ O ₂	0.14	1.39			↑		
56	8.8	-	351.2166	Prostaglandin E2 (PGE2)	C ₂₀ H ₃₂ O ₅	0.17	1.43			↑		
57	19.7	-	365.3408	Nervonic acid	C ₂₄ H ₄₆ O ₂	0.18	1.37			↑		
58	10.1	-	391.2835	Ursodeoxycholic acid	C ₂₄ H ₄₀ O ₄	2.66	1.09	3.26	1.27	↓	↓	↓
59	9.6	-	448.3047	Glycodeoxycholic acid	C ₂₆ H ₄₃ NO ₅	0.37	1.07			↑		
60	8.2	-	464.2993	Glycocholic acid	C ₂₆ H ₄₃ NO ₆	0.39	1.06			↑		
61	12.3	-	464.3121	PE(P-18:0/0:0)	C ₂₃ H ₄₈ NO ₆ P	0.19	1.36			↑		
62	10.9	-	478.2916	LPE(18:1(9Z)/0:0)	C ₂₃ H ₄₆ NO ₇ P	0.31	1.16			↑		
63	8.9	-	495.2937	Pregnanediol 3-O-glucuronide	C ₂₇ H ₄₄ O ₈	10.37	1.68	4.41	1.40	↓	↓	↑
64	11.7	-	522.2813	LPS(18:1)	C ₂₄ H ₄₆ NO ₉ P	0.07	1.80			↑		

UC: ulcerative colitis group, CRC: colorectal cancer group, Con.: control group, FC: Fold change.

Fold1: control group/UC group, Fold 2: control group/CRC group.

VIP1: control group/UC group, VIP2: control group/CRC group.

↑: increased, ↓: decrease.

PTGS2 (5kir) were acquired from the RCSB PDB protein Crystal Structure database (<https://www.pdbus.org/>). PyMOL 2.4 (PyMOL software, Schrödinger, NewYork, NY, USA) was applied to remove water and ligands. AutoDock 4.2.6 (AutoDock software, Scripps Research, La Jolla, CA, USA) was used for hydrogenation and charging. Mol2 structures of key pharmacodynamic ingredients were then obtained from TCMSP (<https://old.tcm-sp-e.com/tcm-sp.php>), and the two receptors were semi-flexibly docked with the active ingredients by AutoDock 4.2.6 (AutoDock software, Scripps Research, La Jolla, CA, USA). In the end, PyMOL 2.4 (PyMOL software, Schrodinger, NY, USA) was used to visualize the molecular docking results.

2.12. Statistical analysis

All calculated experimental values were presented as mean ± SD. Statistical analysis was conducted with Student's t-test using SPSS 26.0 (SPSS software, SourceForge, San Diego, CA, USA).

3. Results

3.1. Composition identification results of GQD in vitro and in vivo

Through analysis of the fragmentation pathways obtained from literature sources and public data, as well as database matching, comparison of mass accuracy, isotope patterns, and retention times of reference standards, 93 and 34 compounds in GQD were preliminarily identified in the positive and negative ion mode, respectively. And a total of 35 components in vivo were detected in GQD. The total ion chromatograms (TICs) were shown in Fig. S1. The specific information of each chemical component was shown in Table 1.

3.2. Network pharmacology predictive analysis

43 targets were obtained in total from the intersection of 35 in vivo component targets (the top 5 targets with the highest Probability value) and disease targets. Then, PPI network diagram of 43 targets was constructed through String database (Fig. 1A). With the degree value > 4 as

the standard, 31 key targets were screened out and the interaction network diagram was drawn (Fig. 1B). The list of targets was shown in Table S6. Finally, using Cytoscape 3.9.1 (UC, San Diego, La Jolla, CA, USA) software, a network diagram of 4 herb, 35 components and 31 targets was constructed (Fig. 1C). The top 4 components with the highest degree of each herb were identified as the key active components that might play important roles in drug efficacy. As a result, Ononin, genistein, puerarin, daidzein were the key components in Pueraria lobata (Willd.) Ohwi (Gegen); Skullcapflavone II, chrysin 7-O-beta-gentiobioside, baicalin, wogonoside were the key components in Scutellaria baicalensis Georgi (Huangqin); DeMethyleneberberine, p-coumaric acid, coptisine, berberine were the key components in Coptis chinensis French (Huanglian); Isoliquiritigenin, glyasperin A, isononin and glycyrrhizin were the key components in Glycyrrhiza uralensis Fisch (Gancao).

3.3. GQD intervention mitigated histopathologic injury in colon tissue caused by UC and CRC and reduce gastrointestinal adverse reactions of XELOX

The colon structure of control group was complete, and goblet cells were arranged neatly (Fig. 2A). However, colonic mucosa ulceration was serious in UC group, and pathological phenomena such as absence of colonic mucosal epithelial cells, destruction of glandular structure and disappearance of crypt structure were found. Severe colon erosion was observed in CRC group, and the pathological features were more obvious than UC group. After GQD treatment, the pathological phenomena of colonic tissue were recovered to a certain extent. Moreover, the colonic lesions of rats treated with GQD combined with XELOX were more improved than those treated with XELOX alone, indicating that GQD could effectively reduce colonic mucosal injury, assist XELOX to enhance the effect of improving intestinal lesions and reduce gastrointestinal adverse reactions of chemotherapy drugs.

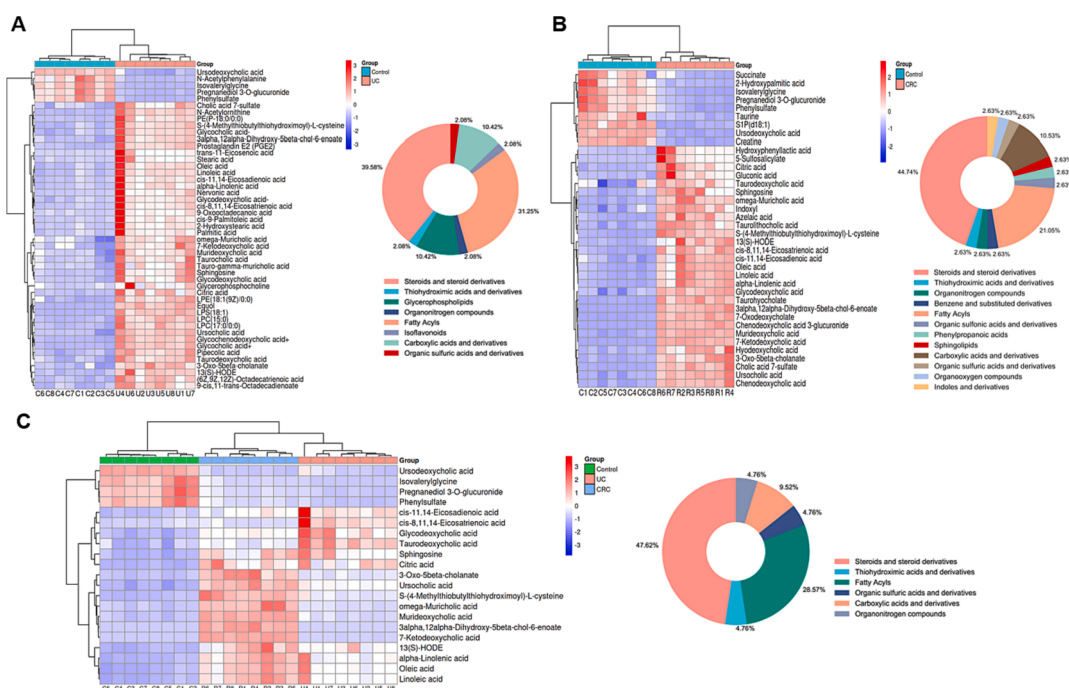


Fig. 6. Heat maps of differential metabolites between the control and UC groups (A); Heat maps of differential metabolites between the control and CRC groups (B); Heat maps of differential metabolites in both the UC and CRC groups (C); circle graphs represented the classification and proportion of differential metabolites.

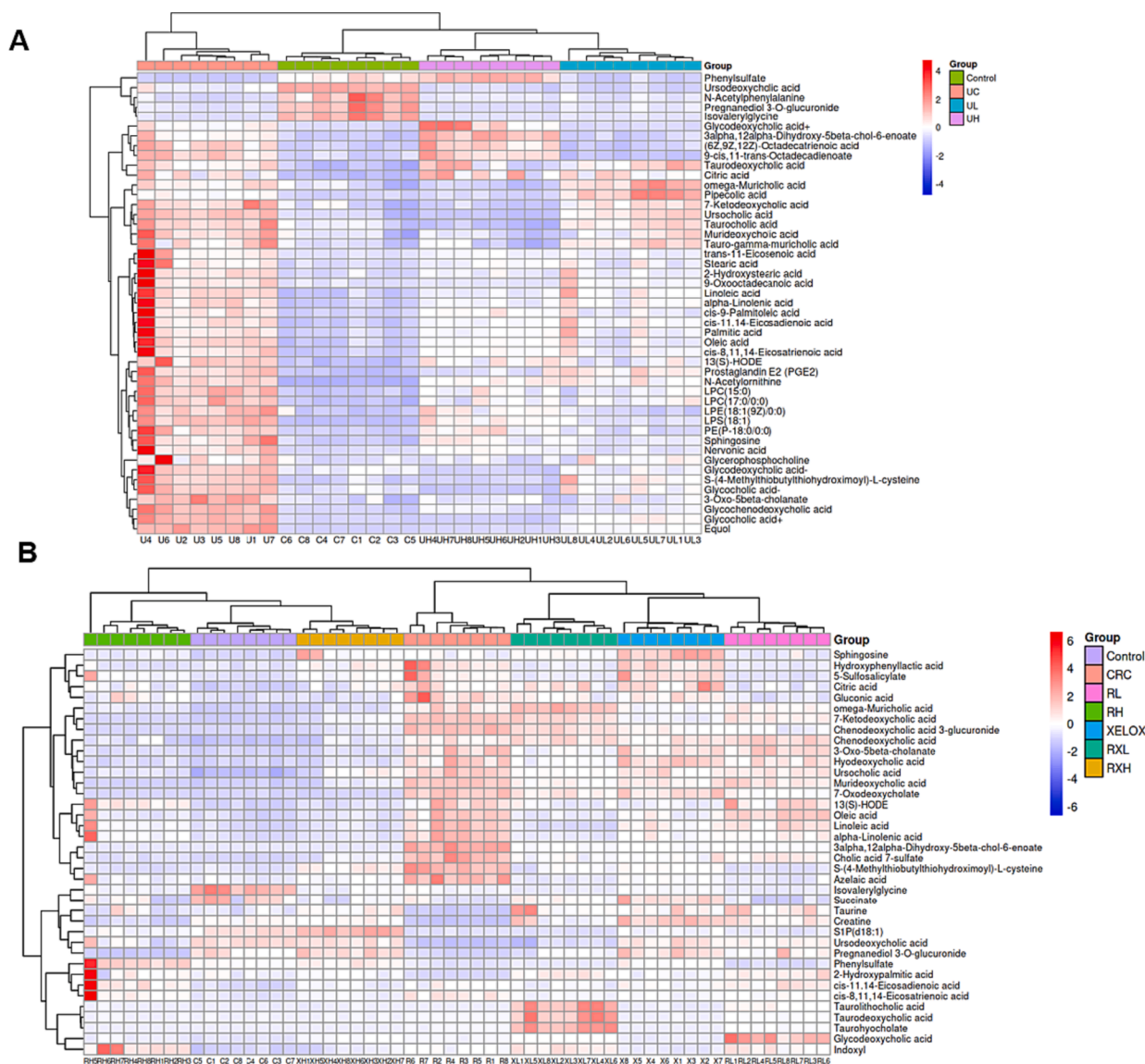


Fig. 7. Heat maps of differential metabolites between the control and UC groups after treatment (A); Heat maps of differential metabolites between the control and CRC groups after treatment (B).

3.4. GQD intervention enhanced anti-inflammatory, antitumor and antioxidant activities

The activities of anti-inflammatory, anti-tumor as well as anti-oxidative of GQD were evaluated by ELISA. As shown in Fig. 2B, the pro-inflammatory factors TNF- α , IL-6 and IL-1 β in colon and serum increased substantially in the development of UC to CRC. After GQD treatment, significant callback effect was observed in both UC and CRC period. Meanwhile, the inflammatory factors in RXL and RXH groups were more significantly decreased than those in XELOX group. In addition, GQD also greatly increased the content of IL-10, the anti-inflammatory factor. And there was a more significant correction trend in the RXL and RXH groups than that in the XELOX group, which declared that GQD had a very strong anti-inflammatory effect, and combined treatment with XELOX might enhance the anti-inflammatory effect. Moreover, the detection results of tumor factor VEGF, antioxidant factor SOD and MDA also proved that GQD had excellent anti-tumor and antioxidant effects, and might assist chemotherapy drugs to enhance its anti-tumor and antioxidant activities. Inflammation and oxidative stress are the key factors in the toxicity and side effects of XELOX. The results above indicated that GQD had great potential in alleviating the toxicity

and side effects of XELOX.

3.5. GQD intervention regulated immune response to resist the adverse reactions of XELOX

It is well known that the balance of the CD4⁺/CD8⁺ is essential for immunomodulatory effects. In this study, CD4⁺ and CD8⁺ positive cells in T lymphocytes were detected by flow cytometry (Fig. 3). The proportion of CD4⁺/CD8⁺ cell subsets in UC and CRC groups were prominently reduced compared with the control group ($p < 0.05$), indicating that inflammation and tumor could damage immune function. However, after GQD intervention, the ratio of CD4⁺/CD8⁺T lymphocytes showed a dose-dependent correction and was similar to that of the control group, enunciating that GQD treatment could normalize the immune system's balance and facilitate to play an anti-tumor role. In addition, after treatment of GQD combined with XELOX, a further reversed trend in the T lymphocytes proportion (CD4⁺/CD8⁺) was found refer to the XELOX treatment group. The data above manifested that the intervention of GQD combined with XELOX could have a positive effect on the immune system's ability to fend off unfavorable reactions.

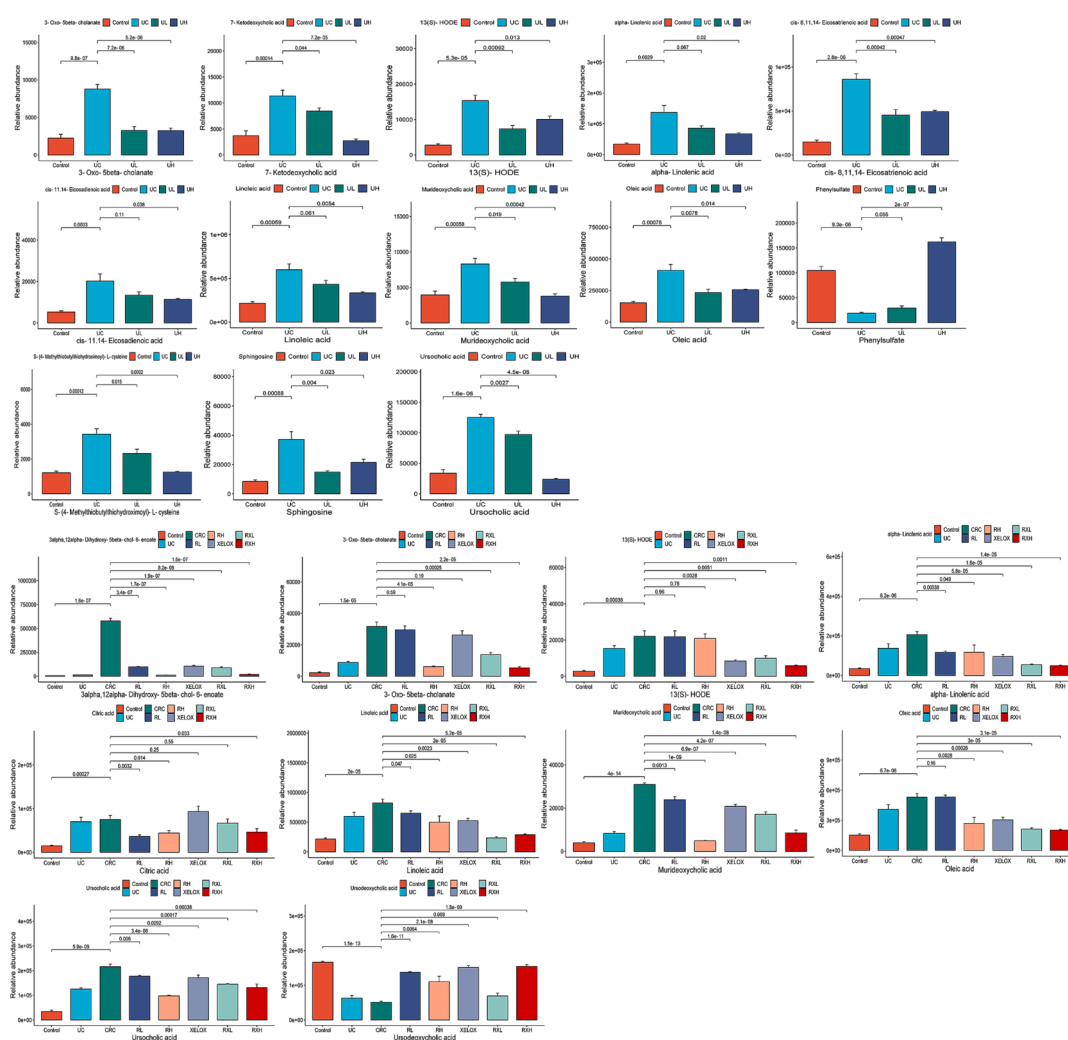


Fig. 8. Column chart of different metabolite concentrations in the control, UC, UL and UH groups (A); Column chart of different metabolite concentrations in the control, UC, CRC, RL, RH, XELOX, RXL and RXH groups (B).

3.6. Intestinal microflora analysis

To study the impacts and molecular underpinnings of the microbial consortia on colorectal carcinogenesis, 16S rDNA sequencing technology was applied to detect the gut microbial community of rats in each group. As shown in Fig. 4A, the community distribution histogram of each group at various levels was drawn. Moreover, LDA distribution histogram and cladogram of dominant microorganisms in different groups were displayed both in Figs. 4 and 5. It could be seen from the diagram that during the evolution from UC to CRC, the intestinal microflora was obviously disturbed, manifested with *Firmicutes*' abundance dramatically dropped, while *Proteobacteria*'s abundance dramatically grew at the phylum level. The microflora with high abundance were *Escherichia_Shigella* and *Lactobacillus*, and the two bacteria were common beneficial bacteria and harmful bacteria in vivo, respectively (genus level). The results showed that from UC to CRC, the abundance of *Escherichia_Shigella* gradually increased, and that of *Lactobacillus* gradually decreased. After GQD intervention, the abundance of various microflora including the above microflora was regulated towards normal levels, indicating that GQD could treat UC and CRC by remodeling intestinal microflora homeostasis and inhibit the progression of UC to CRC. What's more, the decline trend of *Escherichia_Shigella* in RXL and RXH groups was more than that in XELOX group, the *lactobacillus*' abundance in the RXL and RXH groups was much greater than that in XELOX group, suggesting that GQD could help restore the balance of

intestinal microflora on the basis of XELOX treatment.

3.7. Non-targeted metabolomics analysis and correlation analysis with intestinal microflora

To further explore the mechanism of GQD regulation of disease at the small-molecule level, non-targeted metabolomics study was performed on colon samples by HPLC-Q-TOF-MS/MS, with

proven precision, stability, and reproducibility (Table S7). The Control, UC and CRC groups showed significant separation without overfitting (Fig. S2). Subsequently, metabolites satisfying multiple conditions were screened out ($P < 0.05$, $FC > 2.0$ or $FC < 0.5$, $VIP > 1.0$) as potential biomarkers. In the end, 45 biomarkers were screened in the Control and UC groups, and 38 biomarkers were examined in the Control and CRC groups, among which 21 biomarkers were examined in both the UC and CRC groups. The detailed information of each biomarker was shown in Table 2. Then, the abundance of these metabolites in each group was visualized using heat maps (Figs. 6 and 7) to intuitively investigate the variation of metabolites after GQD intervention. Moreover, among the 21 metabolites associated with UC and CRC, linoleic acid, 7-ketodeoxycholic acid and other metabolites showed obvious trend of correction after treatment ($p < 0.05$), and the changes of these metabolites were shown in Fig. 8.

Furthermore, the MetaboAnalyst (<https://www.metabo-analyst.ca/>) platform was used to enrich the KEGG pathway (Fig. 9). The results

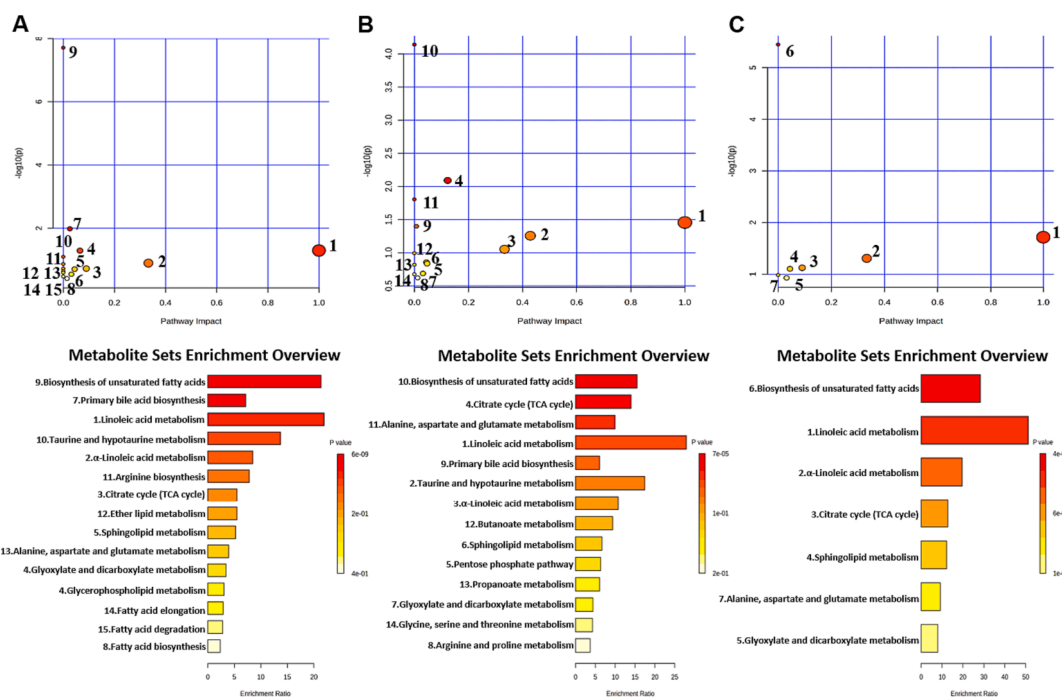


Fig. 9. KEGG enrichment pathway maps of differential metabolites between the control and UC groups (A); KEGG enrichment pathway maps of differential metabolites between the control and CRC groups (B); KEGG enrichment pathway maps of differential metabolites related to UC and CRC (C).

showed that 15 metabolic pathways were significantly enriched during UC development. 14 metabolic pathways were significantly enriched during CRC development. 7 pathways might be affinitive to the transition from UC to CRC.

Whereafter, Spearman correlation analysis was adopted to evaluate the interaction between altered metabolites and microflora, in order to find out the key microflora and metabolites (Fig. 10). According to the Metastats analysis, among the differential microflora in control vs UC and control vs CRC, there were 22 differential microflora both in the UC and CRC groups at phylum and genus level, including *Enterococcus*, *Allobaculum*, *Escherichia Shigella*, *Dubosiella*, *Ligilactobacillus*, *Lactobacillus* etc. And the correlation analysis was performed between them and 21 differential metabolites. The abundance of *Proteobacteria*, *Enterococcus*, *Allobaculum*, *Escherichia Shigella*, *Dubosiella* and *uncultured Clostridiales bacterium* showed a gradually increasing change pattern in the development process from UC to CRC. On the contrary, the abundance of *Marvinbryantia*, *Monoglobu*, *Lachnospiraceae UCG_006*, [*Bacteroides*] *pectinophilus group*, *Gordonibacter*, *Ligilactobacillus* and *Lactobacillus* showed a gradual decrease. The above bacteria were considered to have connections to the evolution of UC into CRC. Correlation analysis showed that *Proteobacteria*, *Escherichia Shigella* and several bacteria had a significant positive correlation with unsaturated fatty acids (oleic acid, alpha-linoleic acid, linoleic acid, etc.). *Ligilactobacillus*, *Lactobacillus* and other bacteria showed significant negative correlation with unsaturated fatty acids.

3.8. Integrated analysis of network pharmacology and metabolomics

Using the Metscape plug-in to form compound-reaction-enzyme-gene networks, 31 crucial targets from network pharmacology results and 21 distinct metabolites from metabolomics results were imported to the Cytoscape 3.10.0 (UC, San Diego, La Jolla, CA, USA) software, to visually related genes and metabolites of interaction (Fig. 11). Six metabolites (linoleic acid, *cis*-8,11,14-eicosatrienoic acid, sphingolipid, α -linoleic acid, oleic acid, citric acid) as well as three targets (ALOX15, CYP1B1, and PTGS2) were identified in the network. Among them, linoleic acid and *cis*-8,11,14-eicosatrienoic acid were key metabolites

that had metabolic relationship with the targets of components *in vivo*. ALOX15 and CYP1B1 were core genes involved in the metabolism of linoleic acid, while ALOX15 and PTGS2 were important genes involved in the metabolism of *cis*-8,11,14-eicosatrienoic acid. These distinct targets and metabolites were chosen as the main metabolites and targets.

3.9. Western blot analysis of ALOX15, CYP1B1 and PTGS2 proteins

As shown in Fig. 12A, ALOX15, CYP1B1, and PTGS2 were all activated ($p < 0.05$) in UC and CRC groups, and each protein in CRC group was expressed more than the UC group. In addition, the expression of ALOX15, CYP1B1, and PTGS2 proteins were effectively inhibited by different concentrations of GQD ($p < 0.05$), especially the higher doses of GQD. Particularly, the administration of GQD combined with XELOX showed a stronger advantage in reversing the expression level of the above proteins than that of XELOX administration alone. These results indicated that the pathogenesis of UC and CRC might be accompanied by the activation of ALOX15, CYP1B1, and PTGS2 proteins, GQD exerted anti-inflammatory and anti-tumor effects by down-regulating these proteins, which was also a key mechanism for GQD to enhance the efficacy of XELOX.

3.10. Molecular docking result

In order to explore the pharmacodynamic substance basis of GQD in the therapy of UC and CRC, molecular docking was conducted between ALOX15, CYP1B1, PTGS2 and active components, respectively. Firstly, the macromolecular ligands of ALOX15 (2p0m), CYP1B1 (3 pm0) and PTGS2 (5kir) were downloaded from the PDB database (<https://www.pdbus.org/>), respectively. Then, the potential active components were semi-flexible docked with the receptor proteins respectively. RS7, BHF and rofecoxib (RCX) were the positive drug of ALOX15, CYP1B1 and PTGS2, which were semi-flexible docked to 2p0m, 3 pm0 and 5kir, respectively. The results showed that GLU357 was the main active sites of 2p0m, GLN332, ASN228 were the main active sites of 3 pm0, and PHE518, ILE517, GLN192, SER530 were the main active sites of 5kir. Moreover, the binding energies to proteins of ononin, genistein,

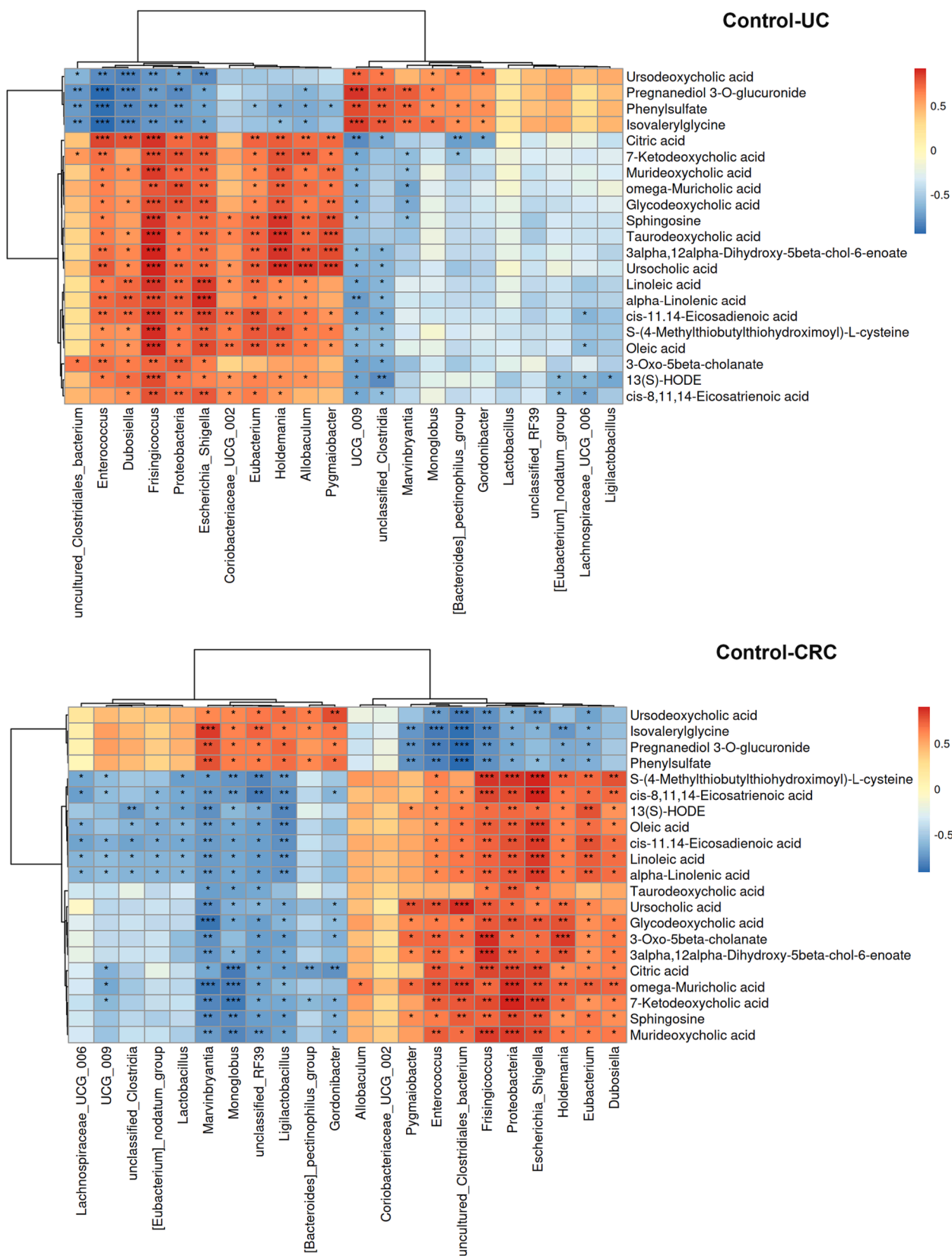


Fig. 10. Correlation heat map of key differential microflora and differential metabolites. *p < 0.05, **p < 0.01, ***p < 0.001.

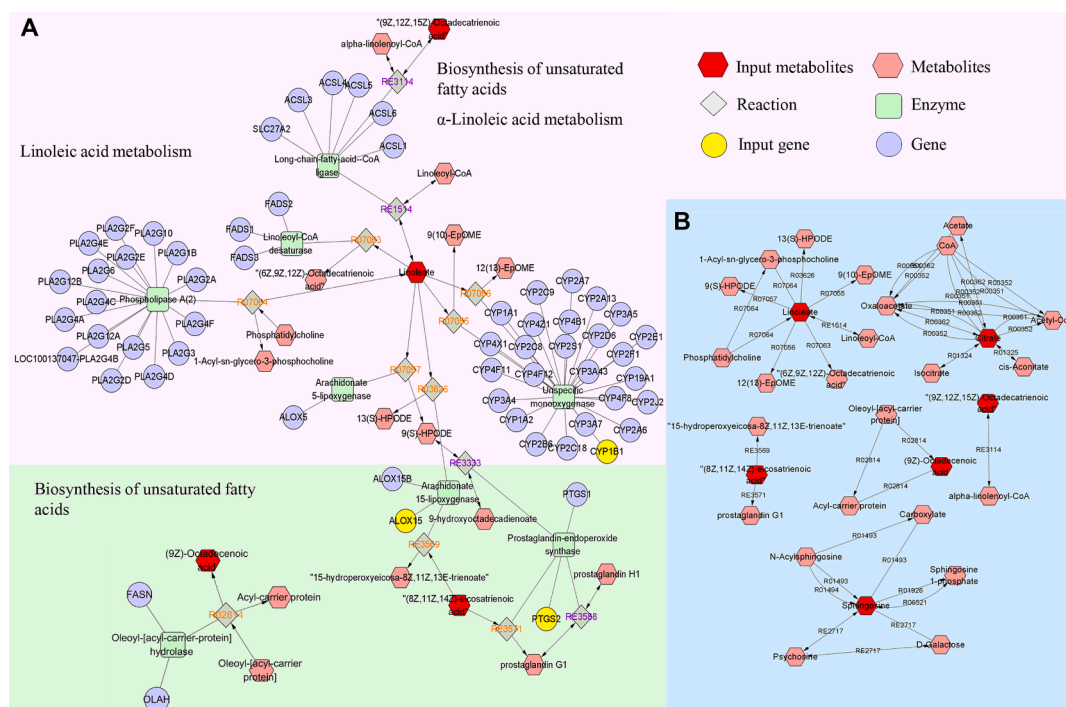


Fig. 11. The compound-reaction-enzyme-gene networks of the key metabolites and targets (A); the network of interactions between key metabolites (B).

puerarin, daidzein, skullcapflavone II, baicalin, wogonoside, p-coumaric acid, coptisine, isoliquiritigenin, glyasperin A were less than -5 kcal/mol and the binding sites were similar to positive drugs, so that the above components were identified as key active components. Details of binding energy were shown in Table S8, and the results of protein–ligand interaction profile were presented in Fig. 12B and Fig. S3-5.

4. Discussion

GQD has been utilized to resist UC and other IBD since ancient times. Although several scholars have explored its therapeutic effect on CRC in recent years, the specific mechanism of action is not very clear (Fan et al., 2020, Liu et al., 2021). Furthermore, as one of the commonly used clinical treatment methods for CRC, XELOX may have certain harmful side effects and lower patients' compliance and quality of life. In clinical practice, Chinese medicine is frequently used in conjunction with chemotherapy drugs to reduce patients' adverse reactions. Our current study was the first to deeply study the pharmacodynamic effect, mechanism of action as well as pharmacodynamic material basis of XELOX combined with GQD in the treatment of CRC. HE staining results suggested that GQD combined with XELOX could effectively reduce intestinal mucosal injury and reduce gastrointestinal adverse reactions. Particularly, the contents of TNF- α , IL-6, IL-1 β , IL-10, VEGF, SOD and MDA were significantly recovered after GQD treatment compared with the disease group ($p < 0.05$), and were close to that of the control group. Therefore, the excellent performance of GQD in assisting XELOX in enhancing anti-inflammatory, antioxidant, anti-tumor and regulating immune function was fully confirmed in this study. Inflammation and oxidative stress are major factors in nerve damage, and the low immune function is the adverse factor that leads to a series of adverse reactions. Therefore, this study suggested that GQD might counteract the toxic side effects and pain response of XELOX by controlling inflammation, oxidative stress, and boosting the immune system.

Altered microflora and metabolites is regarded as one of the most significant hallmarks of gastrointestinal disease (Lanis et al., 2017). 16S rDNA sequencing is a key technology that helps us fully understand the abundance of gut microbiome and its composition. Major advances in

metabolomics technology provide us with tools to reveal the dynamic changes of endogenous metabolites at the level of small molecules in different stages of disease progression (Wu et al., 2020). The results showed that among several bacteria groups with significant increases, *Proteobacteria*, *Allobaculum*, *Escherichia_Shigella*, *Dubosiella* etc. were proved to be potential pathogenic bacteria (Hu et al., 2022, Otake-Kasamoto et al., 2022), and abnormal increases in abundance were detected in a variety of IBD and CRC groups. While *Ligilactobacillus* and *Lactobacillus* are two common beneficial bacteria, which showed a gradual decline in the evolution of inflammation into cancer. The above results indicated that the possible mechanism of UC development into CRC was to destroy the dynamic equilibrium of intestinal micro-environmental environment, decrease the composition of helpful bacteria and increase the composition of harmful bacteria. The abundance of harmful bacteria was sensibly inhibited after GQD intervention, and the abundance of beneficial bacteria was also substantially reversed. In particular, the abundance of *Escherichia_Shigella* and *Lactobacillus* decreased and got higher even more respectively after combined administration. Linoleic acid, oleic acid, 13(S)-HODE and other 21 metabolites were different metabolites found in UC and CRC groups, and the concentrations of these substances showed a trend of gradual increase or decrease from UC to CRC. It is worth noting that after GQD combined with XELOX intervention, the correction trend is stronger than XELOX intervention. The results of correlation analysis showed that several harmful bacteria had strong positive correlation with linoleic acids and unsaturated fatty acid metabolites, but showed opposite relationship with beneficial bacteria such as *Lactobacillus*. It is suggested that the above bacteria and metabolites were deeply related to the development of UC and CRC, and might be used as potential targets for the prevention and control of UC-associated CRC, as well as key targets for the synergistic effect of GQD and XELOX.

The rise of network pharmacology has brought light to the exploration of the mechanism actions of TCM compounds and the development of new therapeutic methods (Qi et al., 2021). The construction of compound-reaction-enzyme-gene network realized the combination of metabolomics and network pharmacology, thus to find the key components that play the drug effect and speculate the possible mechanism of

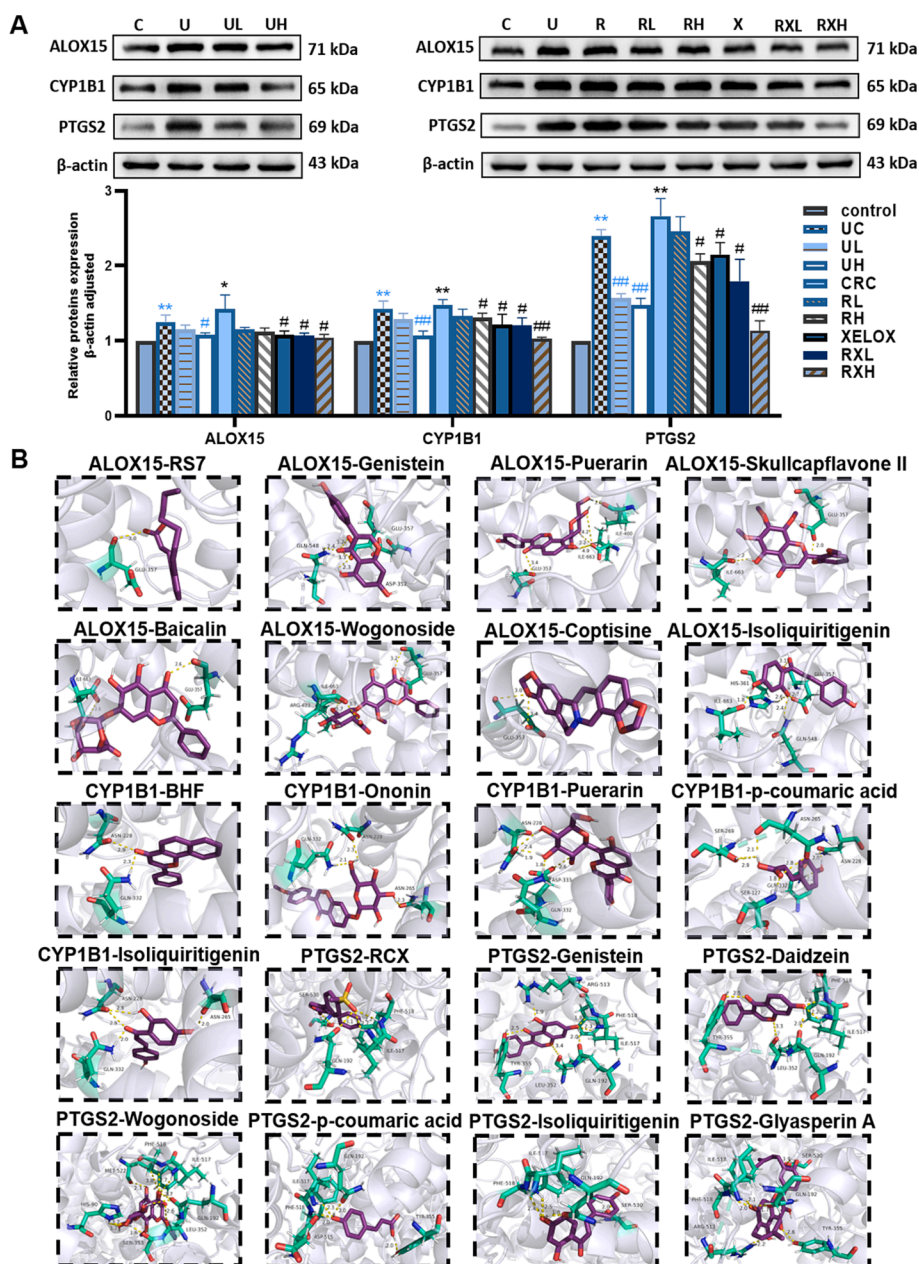


Fig. 12. Typical protein bands and relative expression of ALOX15, CYP1B1 and PTGS2 proteins in western blot analysis; Values shown are means \pm SD. * $p < 0.05$, ** $p < 0.01$ UC vs Control group; * $p < 0.05$, ** $p < 0.01$ CRC vs Control group; # $p < 0.05$, ## $p < 0.01$ vs UC group; # $p < 0.05$, ## $p < 0.01$ vs CRC group (A); Molecular docking interaction diagrams of key active components with macromolecular ligands (B).

action. Molecular docking technique is a kind of simulation method that can visually show the interaction between receptor and drug molecule, which can predict binding patterns and affinity. In recent years, this technique has been widely used by many researchers (Raja et al., 2022, Vennila et al., 2023). In our study, the reliability of the mechanism of action was further verified by western blot and molecular docking, and the core targets and components of the drug effect were clarified. Lipoxygenase arachidonic acid 15 (ALOX15) and Cytochrome P450 1B1 (CYP1B1) are two key lipoxygenase enzymes in the linoleic acid metabolic pathway (Ruparel et al., 2012). Recent research has revealed a link between aberrant ALOX15 expression and a higher risk of multiple tumors and inflammatory disorders. Arachidonic acid was converted to 12-HPETE and 15-HPETE by protease, and 12-HPETE can further be metabolized into a factor with pro-inflammatory properties (Kulkarni et al., 2021). In addition, ALOX15 can also oxidize arachidonic acid and increase lipid peroxidation, resulting in oxidative cell death (Xu et al.,

2021). Linoleic acid and arachidonic acid are two examples of polyunsaturated fatty acids that are extensively processed by the cytochrome P450 (CYP) family (Luo and Liu, 2020). Previous studies have shown that CYP1B1 protein has been overexpression in cancer cells, and this process was closely related to tumor growth (Chen et al., 2023). Down-regulating the expression of CYP1B1 could prohibit the multiplication and migration of CRC cells (Patel et al., 2014). Prostaglandin endoperoxide synthase2 (PTGS2), also known as COX-2, is involved in controlling of pathological reactions like inflammation and tumor (Kunzmann et al., 2013). PTGS2 can catalyze the metabolic process of arachidonic acid, thus producing proinflammatory prostaglandin E2 and other substances, thereby enhancing the invasion potential of tumor cells, etc (Vene et al., 2020). Therefore, PTGS2 is usually highly expressed in inflammatory and malignant tumor tissues (Hidalgo-Estevez et al., 2020). Western blot results showed that the expressions of ALOX15, CYP1B1 and PTGS2 proteins of UC and CRC groups were abnormally

increased, and their expressions were inhibited by GQD. After combined treatment with XELOX and GQD, the expression levels of the three proteins were more reversed to those of the control group. These trends confirmed that ALOX15, CYP1B1 and PTGS2 proteins played a major role in the pathogenesis of UC and CRC. Abnormal increase in the expression level of these proteins can lead to increased inflammation and thus increase the risk of CRC. Moreover, GQD regulated linoleic acid and unsaturated fatty acids metabolism by inhibiting overexpression of ALOX15, CYP1B1 and PTGS2. The changes of metabolites might adjust the structure of the microflora and thus affect the progression of the disease, which is also the key mechanism of the synergistic anti-tumor effect of GQD and XELOX. And ononin, genistein, puerarin, daidzein, skullcapflavone II, baicalin, wogonoside, p-coumaric acid, coptisine, isoliquiritigenin, gylasperin A were the key active components of GQD. All these results served as a crucial benchmark for the creation of novel, efficient, and secure therapy regimens in clinic.

5. Conclusions

Taken together, network pharmacology technology was applied to analyze the components, targets, biological functions of GQD in our study. As a result, the mechanism of prevention and therapy of UC to CRC as well as the ways in which GQD assisting XELOX to treat diseases were excavated. Our outcomings showed that the regulatory effects of XELOX on inflammation, tumor, immune and oxidative stress could be enhanced by GQD. In addition, 16S rDNA sequencing technology and metabolomics results also revealed that GQD combined with XELOX had a unique advantage over XELOX therapy alone in regulating changes in intestinal microbiota and metabolic profile induced by UC and CRC. Ultimately, the key targets and primary ways of GQD were predicted by association analysis of metabolomics with network pharmacology, and the hypothesized mechanism of action was verified by western blot and molecular docking. According to our research, the efficacy of XELOX in the treatment of CRC was effectively increased by GQD. This means that it is possible to reduce the dose of XELOX on the basis of maintaining or even enhancing the efficacy of XELOX, thereby reducing the toxic side effects caused by chemotherapy intervention. Overall, our research offered a fresh perspective on the application of GQD in combination with XELOX to improve patients' quality of life and compliance.

Funding

This work was supported by the National Natural Science Funds of China (Grant No. 81973464/H3203; 8210142956/H3203; 8210132176/H3410), Liaoning Distinguished Professor Project for Qing Li (2017), Shenyang Science and Technology Innovation Project for Young and Middle-aged Talents (RC190505), the project is sponsored by Liaoning BaiQianWan Talents Program in 2019 (A-37), Basic Research Project of Colleges and Universities of Education Department of Liaoning Province (LJKZ0929), Basic Research Project of Colleges and Universities of Education Department of Liaoning Province (LJKQ Z2021033).

CRedit authorship contribution statement

Qi Tang: Writing – original draft, Data curation. **Juan Xie:** Writing – original draft, Data curation. **Xinran Jiang:** Writing – original draft, Data curation. **Mingming Wang:** Investigation, Methodology. **Wei Guo:** Investigation, Methodology. **Chen Liang:** Validation, Data curation. **Xin Jiang:** Investigation, Methodology. **Qing Li:** Resources.

Declaration of competing interest

The authors declare that they have no known competing financial interests or personal relationships that could have appeared to influence the work reported in this paper.

Appendix A. Supplementary material

Supplementary data to this article can be found online at <https://doi.org/10.1016/j.arabjc.2024.105625>.

References

- Cao, Z., Zeng, Z., Wang, B., Liu, C., Liu, C., Wang, Z., Li, S., 2021. Identification of potential bioactive compounds and mechanisms of GegenQinlian decoction on improving insulin resistance in adipose, liver, and muscle tissue by integrating system pharmacology and bioinformatics analysis. *J. Ethnopharmacol.* 264, 113289 <https://doi.org/10.1016/j.jep.2020.113289>.
- Chen, C. C., Yang, Y. B., Guo, Y. G., He, J. S., Chen, Z. Y., Qiu, S. H., Zhang, Y. R., Ding, H., Pan, J. H. and Pan, Y. L., 2023. CYP1B1 inhibits ferroptosis and induces anti-PD-1 resistance by degrading ACSL4 in colorectal cancer. *Cell Death Dis.* 14, 271. <https://doi.org/ARTN 271 10.1038/s41419-023-05803-2>.
- Eaden, J.A., Abrams, K.R., Mayberry, J.F., 2001. The risk of colorectal cancer in ulcerative colitis: a meta-analysis. *Gut* 48, 526–535. <https://doi.org/10.1136/gut.48.4.526>.
- Fan, Q., Guo, L., Guan, J., Chen, J., Fan, Y., Chen, Z., Li, H., 2020. Network pharmacology-based study on the mechanism of gegen qinlian decoction against colorectal cancer. *Evid. Based Complement. Alternat. Med.* 2020, 8897879. <https://doi.org/10.1155/2020/8897879>.
- Grivennikov, S.I., 2013. Inflammation and colorectal cancer: colitis-associated neoplasia. *Semin. Immunopathol.* 35, 229–244. <https://doi.org/10.1007/s00281-012-0352-6>.
- Hidalgo-Estevez, A. M., Stamatakis, K., Jimenez-Martinez, M., Lopez-Perez, R., Fresno, M., 2020. Cyclooxygenase 2-regulated genes an alternative avenue to the development of new therapeutic drugs for colorectal cancer. *Front. Pharmacol.* 11, 533. <https://doi.org/ARTN 533 10.3389/fphar.2020.00533>.
- Hu, J., Cheng, S. J., Yao, J. Y., Lin, X. T., Li, Y. C., Wang, W. X., Weng, J. R., Zou, Y. F., Zhu, L. X. and Zhi, M., 2022. Correlation between altered gut microbiota and elevated inflammation markers in patients with Crohn's disease. *Front Immunol.* 13, 947313. <https://doi.org/ARTN 947313 10.3389/fimmu.2022.947313>.
- Khan, I., Ullah, N., Zha, L., Bai, Y., Khan, A., Zhao, T., Che, T., Zhang, C., 2019. Alteration of gut microbiota in inflammatory bowel disease (IBD): cause or consequence? IBD treatment targeting the gut microbiome. *Pathogens*, 8, 126. <https://doi.org/10.3390/pathogens8030126>.
- Kulkarni, A., Nadler, J. L., Mirmira, R. G. and Casimiro, I., 2021. Regulation of tissue inflammation by 12-lipoxygenases. *Biomolecules*, 11, 717. <https://doi.org/ARTN 717 10.3390/biom11050717>.
- Kunzmann, A.T., Murray, L.J., Cardwell, C.R., McShane, C.M., McMenamin, U.C., Cantwell, M.M., 2013. PTGS2 (Cyclooxygenase-2) expression and survival among colorectal cancer patients: a systematic review. *Cancer Epidemi. Biomar.* 22, 1490–1497. <https://doi.org/10.1158/1055-9965.Epi-13-0263>.
- Lanis, J.M., Kao, D.J., Alexeev, E.E., Colgan, S.P., 2017. Tissue metabolism and the inflammatory bowel diseases. *J. Mol. Med.* 95, 905–913. <https://doi.org/10.1007/s00109-017-1544-2>.
- Li, X., Zhang, C., Hui, H., Tan, Z., 2021a. Effect of Gegenqinlian decoction on intestinal mucosal flora in mice with diarrhea induced by high temperature and humidity treatment. *3. Biotech* 11, 83. <https://doi.org/10.1007/s13205-020-02628-0>.
- Li, X., Zhang, C., Tan, Z., Yuan, J., 2021b. Network pharmacology-based analysis of Gegenqinlian decoction regulating intestinal microbial activity for the treatment of diarrhea. *Evid. Based Complement. Alternat. Med.* 2021, 5520015. <https://doi.org/10.1155/2021/5520015>.
- Liu, X., Fan, Y., Du, L., Mei, Z., Fu, Y., 2021. In Silico and in vivo studies on the mechanisms of Chinese medicine formula (Gegen Qinlian decoction) in the treatment of ulcerative colitis. *Front. Pharmacol.* 12, 665102 <https://doi.org/10.3389/fphar.2021.665102>.
- Liu, C.S., Liang, X., Wei, X.H., Jin, Z., Chen, F.L., Tang, Q.F., Tan, X.M., 2019. Gegen Qinlian decoction treats diarrhea in piglets by modulating gut microbiota and short-chain fatty acids. *Front. Microbiol.* 10, 825. <https://doi.org/10.3389/fmicb.2019.00825>.
- Loftus, E.V., 2005. Inflammatory bowel disease extending its reach. *Gastroenterology* 129, 1117–1120. <https://doi.org/10.1053/j.gastro.2005.07.042>.
- Luo, Y., Liu, J.Y., 2020. Pleiotropic functions of cytochrome P450 monooxygenase-derived eicosanoids in cancer. *Front. Pharmacol.* 11 <https://doi.org/ARTN 580897 10.3389/fphar.2020.580897>.
- Luo, H., Vong, C.T., Chen, H., Gao, Y., Lyu, P., Qiu, L., Zhao, M., Liu, Q., Cheng, Z., Zou, J., Yao, P., Gao, C., Wei, J., Ung, C.O.L., Wang, S., Zhong, Z., Wang, Y., 2019. Naturally occurring anti-cancer compounds: shining from Chinese herbal medicine. *Chin. Med.* 14, 48. <https://doi.org/10.1186/s13020-019-0270-9>.
- Miyachi, E., Kim, S.W., Suda, W., Kawasumi, M., Onawa, S., Taguchi-Atarashi, N., Morita, H., Taylor, T.D., Hattori, M., Ohno, H., 2020. Gut microorganisms act together to exacerbate inflammation in spinal cords. *Nature* 585, 102–106. <https://doi.org/10.1038/s41586-020-2634-9>.
- Nishida, A., Inoue, R., Inatomi, O., Bamba, S., Naito, Y., Andoh, A., 2018. Gut microbiota in the pathogenesis of inflammatory bowel disease. *Clin. J. Gastroenterol.* 11, 1–10. <https://doi.org/10.1007/s12328-017-0813-5>.
- Ordas, I., Eckmann, L., Talamini, M., Baumgart, D.C., Sandborn, W.J., 2012. Ulcerative colitis. *Lancet* 380, 1606–1619. [https://doi.org/10.1016/S0140-6736\(12\)60150-0](https://doi.org/10.1016/S0140-6736(12)60150-0).
- Otake-Kasamoto, Y., Kayama, H., Kishikawa, T., Shinzaki, S., Tashiro, T., Amano, T., Tani, M., Yoshihara, T., Li, B., Tani, H., Liu, L., Hayashi, A., Okuzaki, D., Motooka, D., Nakamura, S., Okada, Y., Iijima, H., Takeda, K., Takehara, T., 2022. Lysophosphatidylserines derived from microbiota in Crohn's disease elicit

- pathological Th1 response. *J. Exp. Med.* 219, 10.1084/jem.20211291. <<https://doi.org/ARTN e20211291>>.
- Patel, S.A.A., Bhambra, U., Charalambous, M.P., David, R.M., Edwards, R.J., Lightfoot, T., Boobis, A.R., Gooderham, N.J., 2014. Interleukin-6 mediated upregulation of CYP1B1 and CYP2E1 in colorectal cancer involves DNA methylation, miR27b and STAT3. *Brit. J. Cancer.* 111, 2287–2296. <https://doi.org/10.1038/bjc.2014.540>.
- Qi, X., Xu, H., Zhang, P., Chen, G., Chen, Z., Fang, C., Lin, L., 2021. Investigating the mechanism of scutellariae barbata herba in the treatment of colorectal cancer by network pharmacology and molecular docking. *Evid. Based Complement. Alternat. Med.* 2021, 3905367. <https://doi.org/10.1155/2021/3905367>.
- Quidde, J., Pan, Y., Salm, M., Hendi, A., Nilsson, S., Oechsle, K., Stein, A., Nestoriuc, Y., 2018. Preventing adverse events of chemotherapy by educating patients about the nocebo effect (RENNO study) - study protocol of a randomized controlled trial with gastrointestinal cancer patients. *BMC Cancer* 18, 916. <https://doi.org/10.1186/s12885-018-4814-7>.
- Raja, G., Venkatesh, G., Al-Otaibi, J. S., Vennila, P., Mary, Y. S., Sixto-López, Y., 2022. Synthesis, characterization, molecular docking and molecular dynamics simulations of benzamide derivatives as potential anti-ovarian cancer agents. *J. Mol. Struct.* 1269. <https://doi.org/ARTN 133785 10.1016/j.molstruc.2022.133785>.
- Rodriguez, G., Utate, M.A., Joseph, G., St Victor, T., 2017. Oral chemotherapy adherence: a novel nursing intervention using an electronic health record workflow. *Clin. J. Oncol. Nurs.* 21, 165–167. <https://doi.org/10.1188/17.CJON.165-167>.
- Rogler, G., 2014. Chronic ulcerative colitis and colorectal cancer. *Cancer Lett.* 345, 235–241. <https://doi.org/10.1016/j.canlet.2013.07.032>.
- Ruparel, S., Green, D., Chen, P., Hargreaves, K. M., 2012. The cytochrome P450 inhibitor, ketoconazole, inhibits oxidized linoleic acid metabolite-mediated peripheral inflammatory pain. *Mol. Pain.* 8, p. 73. <https://doi.org/Artn 73 10.1186/1744-8069-8-73>.
- Rutter, M.D., Riddell, R.H., 2014. Colorectal dysplasia in inflammatory bowel disease: a clinicopathologic perspective. *Clin. Gastroenterol. Hepatol.* 12, 359–367. <https://doi.org/10.1016/j.cgh.2013.05.033>.
- Shi, D.F., Liu, L.X., Li, H.B., Pan, D.B., Yao, X.J., Xiao, W., Yao, X.S., Yu, Y., 2022. Identifying the molecular basis of Jinhong tablets against chronic superficial gastritis via chemical profile identification and symptom-guided network pharmacology analysis. *J. Pharm. Anal.* 12, 65–76. <https://doi.org/10.1016/j.jpha.2021.01.005>.
- Shinji, S., Yamada, T., Matsuda, A., Sonoda, H., Ohta, R., Iwai, T., Takeda, K., Yonaga, K., Masuda, Y., Yoshida, H., 2022. Recent advances in the treatment of colorectal cancer: a review. *J. Nippon Med. Sch.* 89, 246–254. <https://doi.org/10.1272/jnms.JNMS.2022.89-310>.
- Siegel, R.L., Miller, K.D., Fuchs, H.E., Jemal, A., 2022. Cancer statistics, 2022. *Ca-Cancer J Clin.* 72, 7–33. <https://doi.org/10.3322/caac.21708>.
- Sun, Q., He, M., Zhang, M., Zeng, S., Chen, L., Zhao, H., Yang, H., Liu, M., Ren, S., Xu, H., 2021. Traditional Chinese Medicine and colorectal cancer: implications for drug discovery. *Front. Pharmacol.* 12, 685002 <https://doi.org/10.3389/fphar.2021.685002>.
- Vene, R., Costa, D., Augugliaro, R., Carlone, S., Scabini, S., Pattacini, G. C., Boggio, M., Zupo, S., Grillo, F., Mastracci, L., Pitto, F., Minghelli, S., Ferrari, N., Tosetti, F., Romairone, E., Mingari, M. C., Poggi, A. and Benelli, R., 2020. Evaluation of glycosylated PTGS2 in colorectal cancer for NSAIDS-based adjuvant therapy. *Cells-Basel.* 9, p. 683. <https://doi.org/ARTN 683 10.3390/cells9030683>.
- Vennila, P., Al-Otaibi, J.S., Venkatesh, G., Mary, Y.S., Raj, V., Acharjee, N., Tamilselvi, P., 2023. Structural, Spectral, Molecular Docking, and Molecular Dynamics simulations of phenylthiophene-2-carboxylate compounds as potential anticancer agents. *Polycycl. Aromat. Comp.* <https://doi.org/10.1080/10406638.2023.2172052>.
- Wang, Z.J., Wang, X.H., Li, J., Zheng, S.H., Zhang, F.P., Hao, S.L., Wang, X.X., Liu, L.K., 2021. The efficacy and safety of modified Gegenqinlian Fomular for advanced colorectal cancer (damp heat accumulation type): a multicenter randomized controlled trial. *Medicine (Baltimore)* 100, e27850. <https://doi.org/10.1097/MD.0000000000027850>.
- Wu, J.W., Wei, Z.H., Cheng, P., Qian, C., Xu, F.M., Yang, Y., Wang, A.Y., Chen, W.X., Sun, Z.G., Lu, Y., 2020. Rhein modulates host purine metabolism in intestine through gut microbiota and ameliorates experimental colitis. *Theranostics.* 10, 10665–10679. <https://doi.org/10.7150/thno.43528>.
- Xu, X., Li, J.Y., Zhang, Y., Zhang, L., 2021b. Arachidonic acid 15-lipoxygenase: effects of its expression, metabolites, and genetic and epigenetic variations on airway inflammation. *Allergy Asthma Immun.* 13, 684–696. <https://doi.org/10.4168/aaair.2021.13.5.684>.
- Xu, L., Zhang, J., Wang, Y., Zhang, Z., Wang, F., Tang, X., 2021a. Uncovering the mechanism of Ge-Gen-Qin-Lian decoction for treating ulcerative colitis based on network pharmacology and molecular docking verification. *Biosci. Rep.* 41, BSR20203565 10.1042/BSR20203565.
- Zheng, D., Liwinski, T., Elinav, E., 2020. Interaction between microbiota and immunity in health and disease. *Cell Res.* 30, 492–506. <https://doi.org/10.1038/s41422-020-0332-7>.
- Zhu, L., Gu, P., Shen, H., 2019. Protective effects of berberine hydrochloride on DSS-induced ulcerative colitis in rats. *Int. Immunopharmacol.* 68, 242–251. <https://doi.org/10.1016/j.intimp.2018.12.036>.
- Zhu, J.Z., Tan, Z.Q., Hollis-Hansen, K., Zhang, Y., Yu, C.H., Li, Y.M., 2017. Epidemiological trends in colorectal cancer in China: an ecological study. *Digest Dis. Sci.* 62, 235–243. <https://doi.org/10.1007/s10620-016-4362-4>.